Visceral mesoderm signaling regulates assembly position and function of the *Drosophila* testis niche

Lauren Anllo and Stephen DiNardo

Perelman School of Medicine at the University of Pennsylvania
The Penn Institute for Regenerative Medicine

Summary

Tissue homeostasis often requires a properly placed niche to support stem cells. The morphogenetic processes that position a niche are just being described. We recently showed that *Drosophila* testis pro niche cells, specified at disparate positions during early gonadogenesis, must assemble in one collective at the gonad anterior. Here, we identify Slit and FGF signals emanating from adjacent visceral mesoderm (Vm) that regulate assembly. In response to signaling, niche cells express *islet*, which we find is also required for positioning the niche. Without signaling, niche cells specified furthest from the anterior are unable to migrate, remaining dispersed. Function of the dispersed niche is severely disrupted, with pro-niche cells evading cell cycle quiescence, compromised in their ability to signal the incipient stem cell pool, and failing to orient stem cell divisions properly. Our work identifies both extrinsic signaling and intrinsic responses required for proper assembly and placement of the testis niche.

Keywords

niche, stem cell, *Drosophila*, testis, visceral mesoderm, *biniou*, Slit, FGF, *islet*

Introduction

Stem cells play a vital role in tissue repair and maintenance, and their loss is associated with degeneration. To maintain stem cells within any tissue, these cells must receive self-renewal signals, often from their resident niche, a microenvironment that supports and directs stem cell behavior (Losick et al., 2011; Moore and Lemischka, 2006; Morrison and Spradling, 2008). Formation of a niche is crucial for stem cell function, and positioning of that niche in the appropriate location during organ development ensures that niche signals remain accessible and confined to stem cells. Regulation of niche assembly is therefore relevant to tissue homeostasis. Both morphogenetic and signaling events that underly formation of tissues where stem cells reside are actively being described in tissues such as the intestinal crypt and the hair follicle (Greicius and

Virshup, 2019; Kaestner, 2019; Martino et al., 2021; Rompalos and Greco, 2014; Shwartz et al., 2020). These tissues and others exhibit a paradigmatic compartmentalization of niche cells during organogenesis. Yet, how niche cells attain the appropriate position within their resident tissue, and signaling that regulates niche location, remain largely unknown.

We study development of the *Drosophila* testis niche, as this niche is well defined and has served as a paradigm for understanding niche-stem cell interactions. Our recent work pioneered live imaging this niche during its formation, which has enhanced its strength as a model system (Anllo et al., 2019; Nelson et al., 2020). Appropriate placement of the niche within the testis is important for polarizing the tissue, and for enabling tissue function (Fuller, 1993; Lee et al., 2008; Tanentzapf et al., 2007). The *Drosophila* testis niche resides at the apex of a closed tube, and directs germline stem cell (GSC) divisions such that differentiating daughter cells are displaced from self-renewal signals. This arrangement facilitates differentiation toward mature sperm as the daughters move further along the tube (Fuller, 1993; Hardy et al., 1979; Kiger et al., 2001; Tulina and Matunis, 2001; Yamashita et al., 2003; Yamashita et al., 2007). Anchorage of the niche at the testis apex ensures proper niche positioning within this tissue throughout the life of the fly. Without anchoring, the niche moves progressively further from the apex, fails to properly orient stem cell divisions, and is eventually lost from the testis (Lee et al., 2008; Papagiannouli et al., 2014; Tanentzapf et al., 2007). Additionally, flies with defects in niche anchoring have reduced fertility (Lee et al., 2008), suggesting the importance of niche position in testis function. While we have some knowledge of how niche positioning is maintained (Anllo et al., 2019; Lee et al., 2008; Papagiannouli et al., 2014; Tanentzapf et al., 2007), how the niche is initially positioned is completely unknown, and is the focus of this work.

The niche assumes its position at the gonad anterior during male embryonic development (Aboim, 1945; Le Bras and Van Doren, 2006; Sheng et al., 2009; Sinden et al., 2012). The embryonic gonad is a spherical organ, comprised of germ cells intermingled with and encysted by somatic gonadal precursor cells (SGPs) (Aboim, 1945; Jenkins et al., 2003). Prior to niche formation, prospective (pro) niche cells are specified from a subset of SGPs by coordination of Notch and EGFR signaling. Notch signaling from nearby tissues promotes niche specification, while EGFR signaling at the gonad posterior suppresses ectopic niche fate (Kitadate and

Kobayashi, 2010; Okegbe and DiNardo, 2011). Properly specified pro niche cells undergo two phases of niche morphogenesis, namely a loose assembly as a cap at the gonad anterior, followed by compaction into a tight, spherical structure (Anllo et al., 2019; Le Bras and Van Doren, 2006). The process by which pro niche cells assemble at the anterior is dynamic. Pro niche cells are initially intermingled with germ cells. They extend protrusions to pull themselves onto the gonad periphery, and then migrate along gonad extracellular matrix (ECM) until they associate in an anteriorly positioned cap (Anllo et al., 2019). This cap assembles at a pole directly opposite a group of male specific somatic cells, msSGPs, that are located at the gonad posterior (Anllo et al., 2019; DeFalco et al., 2003). This arrangement compartmentalizes the niche at the tip of the adult testis. Once assembled at the anterior, the niche displays distinguishing markers of adhesion and gene expression including Fasciclin III (Fas3), E-cadherin (Ecad), and *unpaired* (*upd*) (Le Bras and Van Doren, 2006). Niche formation is complete at the end of embryogenesis, Stage 17 (Anllo et al., 2019; Sheng and Matunis, 2011; Sinden et al., 2012; Tanentzapf et al., 2007)

Our previous live imaging showed that the niche assembles anteriorly, with a reproducible tilt towards interior regions of the embryo (Anllo et al., 2019). This tilt suggested that tissues external to the gonad might be signaling to direct niche placement. The identity of the tissue that directs niche placement, and the signals sent by that tissue, however, were unknown. A few tissues that signal externally to neighboring tissues are located near the assembled niche, including the midgut (Anllo et al., 2019). At this stage in development, the midgut is surrounded by musculature derived from visceral mesoderm (Vm). Vm is a rich signaling center with important roles directing morphogenesis of the underlying endoderm, posterior migration of the salivary glands, and anterior movement of cells that form longitudinal visceral muscles (Azpiazu and Frasch, 1993; Bradley et al., 2003; Cimbora and Sakonju, 1995; Immerglück et al., 1990; Kadam et al., 2012; Tepass and Hartenstein, 1994). We thus hypothesized that Vm tissue is sending signals important for directing anterior assembly of the gonad niche.

Our work here reveals that Vm signaling is required to instruct anterior testis niche assembly. Vm signals Slit and FGF are required to assemble a compartmentalized niche at the gonad anterior. We show that Vm signals are required for anterior movement of pro-niche cells, and for niche cell polarity. We find that in response to

Vm signals, niche cells express the transcription factor *islet*, and *islet* expression is required to assemble the niche. Finally, we show that anterior niche assembly is important for proper niche function and behavior. Taken together, this work unveils how niche position arises during development.

Results

Visceral mesoderm positions the niche.

Our previous live imaging revealed that the niche assembles with a reproducible tilt towards organs at the embryo interior (Anllo et al., 2019), including Vm. To test for a role of the Vm, we examined the position of the niche in gonads dissected from *biniou* mutant embryos, which lack Vm tissue. *biniou* encodes a FoxF transcription factor essential for Vm development, with expression reported solely in Vm precursors (Azpiazu and Frasch, 1993; Zaffran et al., 2001). In sibling controls dissected at the end of embryogenesis when niche morphogenesis is normally complete, we observed a single anterior niche using both Fas3, a cell adhesion marker for niche cell boundaries, and *upd*>GFP, a marker for niche cell-specific gene expression (**Fig1A,C**). Anterior niche position was confirmed relative to msSGPs at the gonad posterior (not shown). In contrast, gonads from *biniou* mutants often exhibited dispersed aggregates of niche cells (**Fig1B,D**). We quantified the number of niche cells and other somatic gonadal precursor cells (SGPs), and observed no differences between *biniou* mutant gonads and sibling controls (**Fig1G**). Thus, the dispersed niche phenotype in *biniou* mutants results not from any change in cell specification, but instead from defects in niche assembly. These data indicate that *biniou* is required for anterior niche assembly, which in turn suggests that the Vm is required to position the niche.

Visceral mesoderm signals are sent before niche assembly.

To investigate the timing of this signaling event, we examined mutants that initially specify the Vm but cannot complete its development. *jelly belly* (*jeb*) mutants specify a subset of Vm precursor cells early in development but lack Vm by Stage 15 (Stute et al., 2004; Weiss et al., 2001). Niche assembly occurs during Stages 15-16 of embryonic development (Anllo et al., 2019). Interestingly, positioning of the niche was normal in *jeb* mutants (**Fig 1H**). Together with what we observe in *biniou* mutants, these results suggest that Vm is dispensable at the

time the niche forms, but is necessary before assembly begins. These findings imply that Vm signals are active before commencement of niche assembly.

We found that at Stage 13 prior to niche assembly, Vm precursor cells (Fas3, white) were in direct contact with SGPs (Traffic jam, red) in both controls and *jeb* mutants (**Fig 1I,J**). While *biniou* mutants occasionally formed Vm precursors (Zaffran et al., 2001), we never observed these residual cells intermingled with SGPs (**Fig S1**). It is likely that early direct cell contacts between pro niche cells and the Vm facilitates the signaling required for niche assembly.

FGF Heartless and Slit signaling promote anterior niche assembly.

biniou was reported to be expressed only in Vm, and only to affect its development (Zaffran et al., 2001). We were surprised to observe some Biniou protein accumulation in SGPs in coalesced gonads (**Fig S3**). We thus sought to confirm a role for the Vm in niche assembly by identifying signals emanating from the Vm that position the niche. We mined existing literature for genes that encoded ligands expressed in Vm tissue. The two FGF ligands, *pyramis (pyr)* and *thisbe* (*ths*), which often act redundantly, met these criteria (Kadam et al., 2012; Stathopoulos et al., 2004). Indeed, *pyr* and *ths* were expressed in Vm cells as reported, and in occasional mesodermal cells outside the gonad but not interspersed among germline cells, which would suggest SGP expression (**Fig S4 A-B, D-E**). When both *pyr* and *ths* were removed, gonadal niche cells were often dispersed (**Fig 2B, E**) or located more posteriorly in the gonad (**Fig 2C, E, see legend**). Consistent with a role for the FGF ligands, mutants of the Heartless FGF Receptor also exhibited niche assembly defects (**Fig S2A-B,E**). It is known that *pyr* and *ths* affect development of a subset of Vm cells, the caudal visceral mesoderm (cvm) (Kadam et al., 2012). However, we found that the cvm was not required for niche placement (**Fig S2C-D**), indicating that the defect in niche assembly observed in *pyr* and *ths* mutants is not due to disruption of cvm. These results demonstrate that FGF Heartless ligands are important for assembling an anterior niche and could emanate from the Vm to do so.

The ligand Slit is also known to be expressed in Stage 13 Vm (Kraut and Zinn, 2004; Rothberg et al., 1990; Sandmann et al., 2006; Soplop et al., 2012), and we confirmed this expression (**Fig S4 B**). There was

occasional expression in mesodermal cells, some of which flank the forming gonad, but not interspersed with germline cells (**Fig S4 C, F**). We next examined *slit* mutants, which do have a partially penetrant defect during an earlier phase of gonad formation (Weyers et al., 2011). For that reason, we limited our analysis to those gonads that completed this earlier morphogenesis phase in *slit* mutants. Indeed, in such mutants quantification revealed niche assembly defects significantly more often compared to sibling controls (**Fig 2D,F**). These data support the idea that Slit, which is expressed in the Vm, contributes to the proper assembly of an anterior gonad niche.

Since the removal of either Slit or the pair of FGF ligands resulted in a partial phenotype, we hypothesized that each of these pathways might independently contribute to niche assembly. Indeed, removing Slit and both FGF ligands resulted in a virtually fully penetrant niche assembly defect compared to depletion for either class of ligand singly (compare **Fig 2H, I** to **Fig 2E and F**). These data support the idea that FGF and Slit signaling act in parallel. Finally, we also observed defects in niche assembly in gonads from embryos heterozygous for *slit, pyr* and *ths* (**Fig S2F-H; see M&M**), suggesting that the dosage of signaling ligands likely emanating from Vm is relevant for proper niche assembly. To summarize, mutants for *biniou*, which have no Vm, exhibit niche assembly defects, and the removal of two classes of signaling ligands, which each appear to emanate from the Vm, exhibit virtually identical niche assembly defects. We conclude that the Vm is the main, if not the only, tissue responsible for positioning the gonadal niche.

Slit and FGF ligands usually direct migratory paths during morphogenesis, and we hypothesized that these ligands might thus be playing a directional role during niche assembly. We examined gonads in which either *slit* or an FGF ligand was overexpressed broadly in the mesoderm (**see M&M**), as overexpression of a directional cue should disrupt niche assembly position. Unfortunately, as has been noted before, *ths* overexpression led to generalized morphogenetic defects (Sun and Stathopoulos, 2018) and impeded gonad formation such that no conclusion could be drawn about it acting as a directional cue (data not shown). In contrast, *slit* overexpression occasionally yielded properly formed gonads. Surprisingly, niche morphogenesis was unaffected in these gonads when compared to sibling controls (**Fig 2G**), suggesting that Slit is acting as a competence and not a directional cue during niche formation.

Visceral mesoderm is required for anterior movement of pro niche cells.

We next sought to ask which step in niche assembly was affected by Vm. Prior to niche assembly, pro niche cells are intermingled with germ cells throughout the gonad. Niche assembly first requires that pro niche cells sort away from the germ cells and onto the gonad periphery (Anllo et al., 2019). Mapping the location of niche cells in Stage 17 gonads showed that in both control and *biniou* mutants, niche cells were located peripherally (**Fig 3G**), suggesting that the Vm is not required for peripheral sorting.

The second step of assembly requires anterior migration of pro-niche cells along the gonad periphery (Anllo et al., 2019). We define anterior migration as the ability of pro niche cells to arrive in their final destination at the gonad anterior at the end of embryogenesis. A properly assembled niche is comprised of some cells specified at the gonad anterior that derive from parasegment (PS) 10, and other cells that are initially specified more centrally in the gonad deriving from PS 11 (Anllo et al., 2019; DeFalco et al., 2008; Le Bras and Van Doren, 2006). We assayed for the ability of pro niche cells to move anteriorly by lineage tracing PS 11 cells. Using *prd*-Gal4 to drive expression of mcd8GFP, shown in magenta, we marked SGPs deriving from PS 11. PS 11 niche cells expressed mcd8GFP (magenta) and Fas3 (green), while PS 10 niche cells were only labeled with Fas3 (green) (**Fig 3A-D**). At the end of embryogenesis, control gonads had anterior PS 11-derived niche cells as expected (**Fig 3A,** arrow**; Fig 3B**). In contrast, PS 11 niche cells in *biniou* mutants mostly remained in their original, more central positions, and were less frequently associated with PS 10 niche cells (**Fig 3C-F).** Taken together, these data suggest that in the absence of the Vm PS 11-derived niche cells failed to reach the gonad anterior, suggesting a requirement for Vm signaling during the second step of niche assembly.

Niche cell polarity is influenced by Vm signaling

Since in the absence of the Vm PS 11 pro niche cells failed anterior migration, and cell migration can rely on cell polarity, we tested whether these cells were properly polarized. In controls, once the normal niche forms, it exhibits enrichments of cytoskeletal and adhesion proteins including E-cadherin (Anllo et al., 2019; Le Bras and Van Doren, 2006). We wondered if these components were asymmetrically distributed within wild type niche cells as assembly completed. Thus, we compared accumulation of F-actin and E-cadherin at niche-GSC

interfaces to niche-niche interfaces. Both proteins were indeed polarized, with F-Actin enriched at niche-GSC compared to niche-niche interfaces, and E-cadherin enriched reciprocally, at niche-niche interfaces (**Fig 4A,B, compared to C,D**). In fact, live imaging the later steps of assembly revealed a dynamic shift in F-actin polarization when pro niche cells began to associate with one another at the gonad anterior. Pro niche cells first exhibited F-actin enrichment along niche-niche interfaces that later re-polarized to niche-GSC boundaries (**Fig 4G**). Quantification of F-actin accumulation in fixed tissue during and after assembly confirmed this shift in polarity (**Fig 4E-F**). These data reveal that polarity is tightly regulated during niche assembly, which aligns with known roles for cell polarity in cell movements and tissue organization. Interestingly, in gonads from *biniou* mutants neither F-actin nor E-cadherin were polarized in niche cells from Stage 17 gonads (**Fig 4H-K**). Similarly, gonads from *fgf* or *slit* mutants also failed to polarized E-cadherin (**Fig 4L-O**). These data support the conclusion that without Vm signaling, niche cell polarity is disrupted, which could suggest a cause for failed anterior migration (see Discussion).

Vm signaling results in *islet* expression in niche cells.

islet encodes a transcription factor that specifies the connectivity and function of subsets of motor neurons through regulation of cell adhesion molecules and axon guidance receptors (Santiago and Bashaw, 2014; Santiago and Bashaw, 2017). We previously showed that *islet* mutants exhibited a dispersed niche phenotype (Anllo et al., 2019) (**Fig 6A-C**), and we note here that this defect is quite similar in severity and penetrance to the defect that we observe in *biniou* mutants, and in *slit, fgf* double mutants (**Fig 1,2**). We now find that Islet protein is significantly enriched in niche cells compared to other SGPs (**Fig 5A,B**). Indeed we also find that a minimal element from the *islet* enhancer region, termed the AMEr (Bataillé et al., 2020; Boukhatmi et al., 2014), was sufficient to drive robust GFP expression in niche cells (**Fig 6D**). Accumulation of Islet protein expression depended on *biniou* (**Fig 5C,D**). Consistent with Slit and FGF ligands acting as important signals emanating from the Vm, *islet* expression was also significantly reduced in niche cells from *slit* or *fgf* mutant gonads compared to niche cells from sibling controls (**Fig 6A-E**). These results suggest that Slit and FGF signals, likely emanating from the Vm, each impact *islet* expression in the niche.

***islet* expression is important for niche cell polarity.**

Because Vm signaling is important for both niche cell polarity and *islet* expression, we wondered whether *islet* was required for polarizing niche cells. *islet* mutant niche cells failed to polarize F-actin, just as in *biniou* mutants (**Fig 6E,** compare to **Fig 4E-F,I**). Since both *biniou*, and *slit* or FGF ligand mutants failed to polarized E-cadherin, we also examined E-cadherin polarization in *islet* mutants. Surprisingly, *islet* mutant niches retained the ability to polarize E-cadherin (**Fig 6F**). Taken together, these results suggest a model whereby Vm signals Slit and FGF promote niche cell assembly by regulating *islet* expression and, separately, influencing E-cadherin polarization (**Fig 6L**, see Discussion).

Without Vm signaling, niche cells are functionally compromised and evade quiescence.

We next tested whether problems with niche assembly affected stem cell regulation by the niche. In the newly formed gonad, the niche recruits nearby germ cells to adopt stem cell fate, orients their divisions, and governs their cell cycling state (Greenspan and Matunis, 2018; Hardy et al., 1979; Sheng et al., 2009; Sinden et al., 2012; Tanentzapf et al., 2007; Voog et al., 2008). One key niche-delivered signal, Upd, is known to activate the Stat pathway to higher levels among the first tier of germline cells adjacent to the niche (Anllo et al., 2019; Kiger et al., 2001; Leatherman and Dinardo, 2010; Leatherman and DiNardo, 2008; Sheng et al., 2009; Tulina and Matunis, 2001). As expected, in control gonads Stat protein was enriched in presumptive GSCs relative to neighboring germline cells (**Fig 7A**). In contrast, Stat enrichment was largely lost in gonads from *biniou* mutants, and from *slit, fgf* double mutants (**Fig 7B-C**). These data suggest strongly that compromised signaling from Vm affects niche function.

Another key aspect of this stem cell niche is that it imposes oriented divisions on GSCs, such that daughter cells are displaced from the niche (Yamashita et al., 2003; Yamashita et al., 2007). In wild type testes, signals from the niche orient GSC divisions perpendicular to the niche-GSC interface (Chen et al., 2018). To accomplish this orientation, one centrosome in the GSC remains near the interface with the niche, while the other duplicated centrosome moves to the opposite pole of the GSC (Sheng et al., 2009; Yamashita et al., 2003) (**Fig 7D**). In contrast, in gonads from *biniou* mutants, both centrosomes in GSCs were often displaced from the interface with the nearby niche cell, suggesting a defect in centrosome anchoring (**Fig 7E,F**). These data again suggest functional defects in the testis niche in the absence of its proper assembly.

Lastly, we tested whether there were alterations in nearby germ cell cycling states by EdU pulse-labeling. The rate of S-phases in GSCs was normal comparing gonads with normally assembled or defective niches (**Fig 7F**). However, whereas normal niche cells are quiescent, gonads with niche assembly defects exhibited many cycling niche cells (**Fig 7I, J**; compare blue to yellow arrows; quantitation in panel **7F**). Thus, without proper assembly, pro niche cells fail to enter cell cycle quiescence.

Taken together, these results show defective niche cell signaling and behavior in the absence of Vm assembly cues, revealing that proper assembly is crucial to function of the testis niche.

Discussion

We have shown here that merely specifying niche cells is not sufficient for that niche to function. To adequately direct stem cell behavior, niche cells must be positioned in an appropriate location in the tissue during organogenesis. Our prior work suggested that an external tissue likely positions the gonadal niche (Anllo et al., 2019), but the identity of that tissue and its directive signals remained completely unknown. Here we reveal the visceral mesoderm (Vm) as the likely tissue required for anterior niche placement, and we elucidate signals expressed in Vm that govern this process. We showed that Vm signals are delivered early in gonadogenesis, and are important for the assembly of pro niche cells into a properly located and functional niche. Our work suggests a model where in response to Vm signals, niche cells express the transcription factor *islet*, which is required to assemble an anterior niche, and to coordinate F actin polarity within that forming structure. Separately, Vm signals are required for E-cadherin polarization in niche cells (see **Fig 6G**). This work identifies signaling, gene expression, and cell biological responses involved in regulating assembly of the testis niche.

Visceral mesoderm regulates development of the testis niche.

We observed a striking and highly penetrant dispersed niche phenotype in the absence of the transcription factor *biniou*. *biniou* is essential for the formation of visceral mesoderm, and its expression had been reported as exclusive to the Vm (Zaffran et al., 2001). However, we observe Biniou accumulation in both the Vm and in

gonadal SGPs (**Fig S3**). While we have not been able to knock down *biniou* in a lineage-specific manner in SGPs, we identify two classes of ligands expressed in Vm and not SGPs, which impact niche development in a manner similar to the global loss of *biniou*. These results suggest strongly that the Vm directs anterior niche formation. Finally, it is notable that Biniou protein accumulation in SGPs was unaffected in *slit, fgf* combined mutants (**Fig S3**), ruling out the possibility that Slit and FGF control niche assembly by regulating *biniou* expression in SGPs.

Our lab recently showed that during niche development, pro-niche cells first extend protrusions to pull themselves out to the gonad periphery, and then move anteriorly to associate, forming an anterior cap on the gonad (Anllo et al., 2019). In *biniou* mutants, niche cells are able to arrive at the gonad periphery, but remain roughly within the region in which they were initially specified (**Fig 3**). Thus, *biniou* expression is required for completion of the second step of niche assembly, anterior association. Niche cells derive from two separate clusters of mesodermal cells that only later associate as one niche (DeFalco et al., 2008; Le Bras and Van Doren, 2006). Pro-niche cells specified in parasegment (PS) 10 mesoderm are already located at what will be the gonad anterior, while those specified in PS 11 must migrate to reach the anterior. The lack of proper assembly in the absence of Vm signaling suggests either that pro niche cells cannot associate properly with other pro niche cells, or they cannot migrate. Our data suggests the latter. Without either *biniou* or the ligands Slit and FGF, we find that pro niche cells can still contact one another, likely as a result of sorting as specified niche cells upregulate adhesion proteins such as Fasciclin3, and E- and N-cadherin (Le Bras and Van Doren, 2006). However, our lineage tracing in *biniou* mutants revealed that PS 11-derived niche cells were almost never located at the gonad anterior (**Fig 3E**). We hypothesize that pro niche cells specified in different gonadal regions are not close enough to sort based on adhesion alone, and require Vm signals to enable movement to form a single niche.

Vm signals are sent well before niche assembly.

In many examples of cell migration, directive signals are active during the morphogenetic event (Montell, 2003; Scarpa and Mayor, 2016). We were surprised to find that the niche assembled normally in embryos that initially

have Vm precursors but lose them prior to that time during which the niche forms (**Fig 1**). From this data, we infer that Vm precursors emit the required signals early, significantly before niche assembly. One possibility is that Vm precursors secrete signals that are retained in extracellular matrix (ECM), and pro niche cells are later exposed to these signals. ECM-scaffolded FGF and Slit have been reported in other systems (Isaacman-Beck et al., 2015; Vlodavsky et al., 1991; Xiao et al., 2011). However, we showed previously that anterior niche cell movement does not rely on interactions with ECM (Anllo et al., 2019), arguing against a role for ECM-scaffolded ligands. Alternatively, early signaling might induce a gene expression program in pro niche cells that enables an appropriate intrinsic cell response later in gonadogensis. Indeed, we showed that before niche assembly, pro niche cells and Vm precursors directly intermingle and that *islet* gene expression is required downstream of Vm signaling. The identification of an *islet* cis-regulatory element sufficient for expression in the niche will help elucidate the circuitry involved in this induction event and establish whether it is a direct response to the signals we define here. Since we show that *islet* is essential in niche assembly, its downstream targets will be of interest. In neurons, targets such as the DCC or Frazzled (Fra) receptor function in directing axons to their appropriate locations (Santiago and Bashaw, 2017). Perhaps such candidates might explain how *islet* induction contributes to niche assembly.

Slit and FGF signals both contribute to niche position.

Our work has identified two signaling pathways that are important for niche assembly and our data suggest that resiliency is built into the niche assembly process. Both the dependence on dosage (**Fig S2**, **2**), and the fact that some niches can assemble in the absence of one pathway (see **Fig 2**) suggest that these pathways cooperate to ensure proper positioning. For example, both pathways might converge on their ability to regulate niche cell polarity, or to induce *islet* mediated gene expression (see **Fig 6**)**.** The contributions of Slit and FGF to niche assembly are reminiscent of the partially overlapping roles of EGFR and PVR in border cell migration during *Drosophila* oogenesis. The immediate downstream effectors of these pathways are unique, yet both EGFR and PVR converge on directing the migratory path of the border cells (Duchek et al., 2001).

In a number of systems, Slit and FGF often function as directional guidance cues (Blockus and Chédotal, 2016; Friedl and Gilmour, 2009; Kadam et al., 2012). Changing the source of the cue in these instances alters

the migratory path of moving cells (Jia et al., 2005; Sutherland et al., 1996). In niche assembly, we tested whether these pathways were acting in this canonical role. While we could not analyze niche formation upon FGF misexpression, we did observe gonads with properly positioned niches upon *slit* misexpression (**Fig 2G**). This result argues that Slit is in fact not acting in its canonical role as a directional cue during niche assembly. Our data instead suggest that Slit is a competence cue acting, for example, to enable pro niche cells to migrate, or licensing responses to as yet unidentified directional signals.

Slit and FGF affect polarity and adhesion in pro niche cells.

If Slit and FGF are eliciting responses prior to niche assembly, it is possible that these signals might regulate modulators of adhesion or the cytoskeleton that are required for the assembly process. Cell movement often relies on proper polarization of cytoskeletal and adhesion proteins (Etienne-Manneville, 2008; Scarpa and Mayor, 2016; Vassilev et al., 2017). We showed that niche cell polarity is normally well-organized during late stages of assembly and in formed niches. However, in the absence of Vm tissue or its ligands, pro niche cells failed to polarize F actin or E-cadherin (**Fig 4**). These data suggest that the niche assembly process depends on proper polarization of pro niche cells, and that Vm signaling enables the organized cell polarity required for anterior niche cell movement. During *Drosophila* gastrulation, FGF signaling has known roles in regulating E-cadherin based cell contacts, and is required to re-establish epithelial polarity in the invaginated mesodermal cells (Clark et al., 2011; McMahon et al., 2010; Sun and Stathopoulos, 2018). These roles are reminiscent of the polarity re-organization we observe during late stages of niche assembly (**Fig 4**), and it is likely that FGF signaling might affect SGPs similarly.

Without proper assembly, niche cells function abnormally and evade quiescence.

Organized placement of a stem cell niche within its resident tissue is a paradigm in stem cell biology. In mammals, intestinal epithelial niche cells are harbored within intestinal crypts, and the dermal papillae niche assembles at the base of the mammalian hair follicle (Wang et al., 2016). The reproducible organization of niche cells during organogenesis suggests that niche assembly might be linked to its ability to function, and our work here reveals evidence of this link. We show that proper assembly of the testis niche is required to activate Jak/Stat signaling in neighboring germ cells, and to orient neighboring stem cell divisions (**Fig 7A-E**), two

distinct consequences of niche signaling. Further, niche cells are known to exhibit cell cycle quiescence in wild types testes (Greenspan and Matunis, 2018; Hardy et al., 1979; Voog et al., 2008), while directing cell divisions of adjacent stem cells (Yamashita et al., 2003). Quiescence is important to the biology of the testis niche, as aberrantly dividing niche cells eventually lead to extraneous niches located away from the testis tip (Greenspan and Matunis, 2018). How niche cells enter quiescence is currently unknown. All embryonic SGPs are in the cell cycle prior to niche formation (Sinden et al., 2012). We find that fully assembled niche cells have withdrawn from cycling (**Fig 7H**), and that niche assembly is a prerequisite for withdrawal from the cycle (**Fig 7H,J**). From these data, it becomes apparent that the paradigmatic organization of niche position is important for niche behavior as well as function.

Tissue homeostasis therefore necessitates that pro niche cells are directed to move to their appropriate position in those instances when they are not initially specified in their final destination. Here, we show that signals from an external tissue result in a gene expression response in pro niche cells, and that response is required to polarize niche cells and enable their movement. That movement results in assembly of a functional niche. Our work shows that proper niche placement is vital for niche function, and identifies a mechanism by which niche cell assembly position is regulated.

Acknowledgements

We would like to thank R. Lehmann, E. Bach, A. Holz, and M. Frasch for sharing antibodies and fly stocks. Stocks obtained from the Bloomington Drosophila Stock Center (NIH P40OD018537) were also used in this study. Special thanks to G. Bashaw, M. Granato, K. Nelson, G. Vida, and B. Warder for their helpful comments on our manuscript.

Author contributions

Conceptualization, L.A. and S.D.; Methodology, L.A. and S.D.; Validation, L.A.; Formal Analysis, L.A.; Investigation, L.A.; Resources, S.D.; Data Curation, L.A. and S.D.; Writing – Original Draft, L.A.; Writing – Review & Editing, L.A. and S.D.; Visualization, L.A.; Supervision, S.D.; Project Administration, L.A. and S.D.; Funding Acquisition, L.A. and S.D.

Declaration of interests

The authors declare no competing interests.

Legends

Figure 1. Visceral mesoderm positions the niche. (**A-D**) Control and *biniou* mutant gonads dissected from Stage 17 embryos. Niche morphogenesis is normally complete by Stage 17 (Anllo et al., 2019; Le Bras and Van Doren, 2006; Sheng et al., 2009; Sinden et al., 2012), resulting in a single aggregate of niche cells at the gonad anterior, opposite in position to the male-specific somatic gonadal precursor cells (msSGPs) that mark the gonad posterior. Control (**A**) and *biniou* mutant (**B**) gonads immunostained with antibodies against Vasa (red) to label germ cells, and Fas3 (white) to label niche cells. (**C-D**) Control (**C**) and *biniou* mutant (**D**) gonads immunostained with Vasa (red) and expressing *upd*-Gal4, UAS-GFP in niche cells (GFP in white). Arrowheads indicate a single niche in control (**A,C**), and dispersed niche cell aggregates in mutant gonads (**B,D**). (**A'-B'**) Fas3 channel alone and (**C'-D'**) GFP channel alone. Dotted lines indicate gonad boundaries. (**E-F**) Quantification of the dispersed niche phenotype in *biniou* mutant gonads, using Fas3 as a marker for niche cell boundaries ($p < 0.001$ Fisher's exact test) (**E**), or *upd*>GFP as a marker for niche cell gene expression ($p = 0.004$ Fisher's exact test) (**F**). Quantitation showed a significant difference between control and either of two null *biniou* alleles. Number of niche cells and non-niche SGPs specified in *biniou* mutant gonads compared to sibling controls (**G**). (**H**) Quantification reveals that niche assembly is not affected in *jeb[weli]* / Df(2R)BSC699 embryos compared to sibling controls. (**I-J**) SGPs that are aggregated in the still-coalescing gonad (Traffic jam, red) are in direct contact with Vm cells (Fas3, white) prior to niche assembly in both control (**I**) and *jeb* mutant embryos (**J**) at Stage 13. Arrows indicate two locations where SGPs (red nuclei) directly contact Vm tissue (white cell boundaries). Scalebars represent 10 um.

Figure S1. *biniou* mutant SGPs do not contact Vm precursors. SGPs (Traffic jam, red) that are still coalescing, and neighboring Fasciclin 3 (Fas3, white) positive Vm tissue in sibling control (**A**) and *biniou[R22]* mutant (**B**) embryos. (**A**) Arrows indicate two SGP nuclei that are directly adjacent to Fas3 positive Vm tissue. In (**B**), there is less Fas3 positive tissue as expected for *biniou* mutants. Arrowheads indicate Fas3 positive Vm tissue that is near the gonad, but not contacting any SGP nuclei. Scale bar represents 20 um.

Figure 2. Slit and FGF signaling are important for niche positioning. (**A-D,H**) Stage 17 gonads immunostained with Vasa antibody to label germ cells (red), Fas3 antibody to label niche cells (white), and Hoechst to label DNA (blue). Dotted line delineates gonad boundaries. Arrowheads indicate niche cell aggregate(s), and asterisk indicates gonad posterior. Scale bar represents 10 um. (**A**) Sibling control gonads have a single anterior niche aggregate. (**B-C**) Df(2R)BSC25 gonads, with a deletion removing the *pyr* and *ths* genes, exhibit niche defects such as dispersed niche aggregates (**B**), and niches that are not at the gonad anterior (**C**). (**D**) *slit[2]* mutant gonads often have dispersed niche aggregates. (**E-G**) Quantification of niche morphogenesis defects in *fgf* ligand ($p = 0.016$, Fisher's exact test) (**E**), *slit[2]* mutant ($p < 0.0001$, Fisher's exact test) (**F**), and Slit overexpression embryos (**G**). (**H**) *fgf*, *slit* multiply mutant gonads exhibit dispersed niches. (**I**) Niche defects in *fgf*, *slit* multiple mutants ($p = 0.003$).

Figure S2. *htl* mutants and *slit*, *fgf* heterozygotes exhibit niche morphogenesis defects. (**A-B**) Stage 17 gonads expressing *six4*-nls-eGFP to mark all SGPs (red) immunostained with Fas3 antibody to label niche cells (white). (**A**) Wild type gonads have a single anterior niche, while (**B**) *htl* receptor mutants exhibit dispersed niche aggregates. (**C,D**) Stage 17 gonads stained with Vasa to label germ cells and E-cadherin to indicate the niche. Both control gonads (**C**) and *hlh54f* cvm mutants (**D**) have anterior niches. **(E,F)** Quantification of niche morphogenesis defects in *htl* mutants ($p = 0.0003$, Fisher's exact test) (**E**) and *slit*, *FGF* heterozygotes ($p = 0.005$, Fisher's exact test) (**F**). (**G-H**) Stage 17 gonads stained with Vasa antibody to label germ cells (red), Fas3 antibody to label niche cells (white), and Hoechst to label DNA (blue). (**E**) Wild type gonads have a single anterior niche, in contrast to (**F**) *slit*, *FGF* heterozygotes which show dispersed niche cells. In all panels, arrowheads indicate niche cells, dotted lines show gonad boundaries, and scale bars represent 10 um.

Figure S3. SGPs express *biniou*. (**A-B**) Stage 16 embryos, and (**C-D**) gonads from stage 16 embryos immunostained with Biniou antibody (white) and Traffic jam to label SGPs (red). SGPs from wild type or *slit, fgf* double mutants express *biniou*. Scale bars are 20 um.

Figure S4. FGF and Slit are expressed in visceral mesoderm. (**A-F**) Embryos fixed and immunostained with Vasa to label germ cells (green), and Fas3 to indicate visceral mesoderm and other tissues, including the overlying epidermis, and the tubular hindgut and foregut (white). (**A,D**) Embryos expressing *pyr*-Gal4 driving

UAS-red Stinger (magenta) to show FGF ligand expression either (**A**) before, or (**D**) during niche assembly. (**A, A'**) Arrowheads show *pyr*-expressing cells within Vm. Arrows reveal a metameric pattern of Pyr in overlying epidermis and more weakly in some underlying mesodermal cells. At this stage SGPs are intermingled with germ cells (green) where little or no Pyr is detectable. (**D, D'**) Pyr is clearly detectable among Vm cells (arrowheads) and the hindgut tube, but not among germ cells (green). (**B,E)** Embryos expressing *ths*-Gal4 driving UAS-red Stinger (magenta) to show expression of the second, redundant FGF ligand. As with *pyr*, we observe expression in the Vm (arrowheads) and some neighboring mesodermal cells (arrows), but not among germ cells (green). (**C,F**) Embryo expressing Slit::GFP (magenta) either (**C**) before, or (**F**) during niche assembly. (**C, C**') Arrowheads indicate clusters of Vm cells expressing Slit::GFP including those near germ cells (green). Slit expression is also observed in cells neighboring the gonad that do not derive from visceral mesoderm. (**F, F'**) Occasional Slit-expressing Vm cells are still present, but little or no expression is detectable among germ cells (green). As expected, Slit is observed on midline glial cells visible in panel F, and associated with hindgut mesoderm (arrows, F'). Scale bars are 20 um.

Figure 3. *biniou* is required for anterior movement of pro niche cells. (**A,C**) Stage 17 dissected gonads expressing mcd8GFP in PS11 cells (magenta), and immunostained with antibodies against Vasa (white) to label germ cells, and Fas3 (green) to label niche cells. (**A**) A control gonad, with a single anterior niche (left, green) containing cells deriving from both PS 10 (green alone, asterisk) and PS 11 (magenta and green, arrow). (**C**) *biniou[R22]* mutant gonads with dispersed niche aggregates (green). Anterior niche cells deriving from PS 10 (green alone, asterisk) do not associate with PS 11 derived niche cells (magenta and green, arrows). Ectopic PS11 niche cells were distinguishable from PS13 msSGPs because msSGPs do not express the niche marker, Fas3 (**B,D**) Cartoons illustrating the distribution of PS11 niche cells in control (**B**) and *biniou* mutant (**D**) gonads, with germ cells in white, PS 10 and PS 12 SGPs in green, and PS 11 and PS 13 SGPs in magenta. (**E-G**) Quantifications comparing *biniou* mutant and sibling control gonads by how often (**E**) PS 11 derived niche cells are located at the gonad anterior ($p < 0.0001$, Fisher's exact test), (**F**) PS 11 niche cells contact anterior PS 10 niche cells ($p < 0.0022$, Fisher's exact test), and (**G**) niche cells are located within 2 microns of the gonad periphery. Scale bars represent 10 um.

Figure 4. Niche cell polarity depends on Vm. (**A**) Niche cells in Stage 17 gonads expressing a somatic cell F actin label, *six4*-eGFP::moesin. (**B**) Quantification of normalized F actin fluorescence intensity at niche-niche interfaces compared to niche-GSC interfaces. Assembled niche cells upregulate F actin at niche-GSC interfaces ($p < 0.0001$, Mann-Whitney test). (**C**) Stage 17 dissected gonads immunostained with an antibody against E-cadherin. (**D**) Quantification of E-cadherin. Assembled niche cells upregulate E-cadherin at niche-niche interfaces compared to niche-GSC interfaces ($p < 0.0001$, Mann-Whitney test). (**E,F**) Quantification of F actin accumulation at niche-niche or niche-germ cell interfaces during (**E**) and after completion (**F**) of niche assembly in fixed tissue ($p < 0.0001$, Wilcoxon test). (**G**) Stills from a time-course of a gonad expressing *six4*-eGFP::moesin to label F actin in all SGPs. F-actin accumulates at niche-niche interfaces when niche cells begin to associate (arrow), and F-actin later reorganizes to accumulate at niche-stem cell interfaces (asterisk). (**H**, **J**) Niche cells from Stage 17 *biniou* mutant gonads expressing *six4*-eGFP::moesin (**H**) or immunostained with an antibody against E-cadherin (**J**). (**I,K**) Quantification of the loss of polarization of F-Actin (**I**) and E-cadherin (**J**) in Stage 17 *biniou* mutant gonads. Niche cell-GSC interfaces are indicated with asterisks, and niche cell-niche cell interfaces are shown with arrows. (**L,M**) Niche aggregates in *fgf* (**L**) or *slit* (**M**) mutant gonads immunostained with E-cadherin antibody (white). A niche-niche boundary (arrow) and niche-GSC boundary (asterisk) is shown for an example niche cell. (**N,O**) Quantification of E-cadherin accumulation at niche-niche (n-n) or niche-GSC (n-g) interfaces in *fgf* **(N)** or *slit* (**O**) mutant gonads compared to sibling controls (WT) (Mann Whitney tests). Scale bars represent 5 um.

Figure 5. Niche cells express *islet* in response to Vm signals. (**A,C**) Stage 17 *six4nls*GFP gonads immunostained with antibodies against GFP (green) to label SGPs and other mesoderm, Fas3 (white) to visualize niche cells, and Islet (red). (**A**) Control gonads express Islet in the niche, while (**C**) *biniou* mutant gonads do not. (**B,D**) Quantification of Islet antibody fluorescence intensity in Fas3 positive niche cells, compared to other non-niche SGPs in (**B**) control ($p < 0.0001$, Mann Whitney test) and (**D**) *biniou* mutant gonads. (**E-G**) Stage 17 gonads immunostained with antibodies against Islet (white), Fas3 (red) to label the niche, and Vasa for germ cells (not shown). Gonad boundaries are delineated with white dotted lines.

Arrowheads indicate niche cells. (**H-I**) Quantification of Islet expression in niche cells from *fgf* (**H**) and *slit* (**I**) mutants, compared to sibling control niche cells ($p < 0.0001$, Mann Whitney test). Scale bars represent 10 um.

Figure 6. *islet* is required for niche assembly and polarity. (**A**) Control and (**B**) *islet* mutant Stage 17 gonads immunostained with Vasa (red) to label germ cells, Fas3 (white) to indicate niche cells, and Hoechst to show all nuclei. (**C**) Quantification of the dispersed niche phenotype in *islet* mutant gonads compared to sibling controls ($p = 0.024$, Mann Whitney test). (**D**) A wild type gonad expressing GFP driven by the *islet* AMEr enhancer element, showing GFP expressed in the niche. Immunostaining reveals germ cells with Vasa (red) and niche cells with Fas3 (white). (**E**) Quantification of F actin accumulation at niche cell interfaces in *islet* mutants with disorganized niche cells. (**F**) Quantification of E-cadherin accumulation at niche-niche (n-n) or niche-GSC (n-g) interfaces in *islet* mutant gonads compared to sibling controls (WT) (Mann Whitney tests). (**G**) A model illustrating how Vm signals influence niche assembly. In all panels, arrowheads indicate niche cells, dotted lines delineate gonad boundaries, and scale bars represent 10 um.

Figure 7. Without the Vm, niches exhibit abnormal function and behavior. (**A-B**) Stage 17 dissected gonads immunostained with antibodies against Stat (white), Fas3 to label niche cells (red), and Vasa to indicate germ cells (not shown). A niche cell is indicated with an asterisk, GSCs with blue dotted lines, and neighboring germ cells with yellow dotted lines. (**C**) Quantification of Stat accumulation in GSCs relative to neighboring germ cells in *biniou* or *slit, fgf* mutants and sibling controls. (**D-E**) Stage 17 gonads dissected and immunostained against Gamma Tubulin (green) to label centrosomes, Fas3 to label niche cell membranes (white), and Vasa to label germ cells (magenta). Arrowheads show GSC centrosomes, and asterisks mark neighboring niche cells. (**F**) GSCs with centrosomes near a GSC-niche interface compared in control and *biniou* mutant gonads (**G-H**) Quantification of the percentage of GSCs incorporating EdU (**G**), and (**H**) the percentage of gonads with quiescent niches. (*** $p = 0.0001$, ** $p = 0.004$, Fisher's exact test). (**I-J**) Stage 17 gonads dissected, exposed to an EdU pulse, and immunostained. EdU nuclear label is shown in white, Fas3 niche membrane marker in magenta, and Vasa germ cell marker in green. A control niche cell with no EdU incorporation is indicated with a blue arrow, and a *biniou* mutant niche cell incorporating EdU is indicated with a yellow arrow. Blue asterisk denotes a cycling GSC. Scale bars are 10 um.

Methods

RESOURCE AVAILABILITY

Lead contact

- Further information and requests for resources and reagents should be directed to and will be fulfilled by the lead contact, Stephen DiNardo (sdinardo@pennmedicine.upenn.edu).

Materials availability

- This study did not generate new unique reagents.

Data and code availability

- All data reported in this paper will be shared by the lead contact upon request.
- This paper does not report original code.
- Any additional information required to reanalyze the data reported in this paper is available from the lead contact upon request.

EXPERIMENTAL MODEL AND SUBJECT DETAILS

Drosophila Stocks

All *Drosophila* lines used are listed in the Key Resources Table (KRT). *slit[2]* is a null allele with no detectable protein product (Battye et al., 2001; Nusslein-Volhard et al., 1984). To remove *pyr* and *ths* together, we used a small chromosomal deficiency, Df(2R)BSC25, which completely deletes the genes encoding both ligands (Stathopoulos et al., 2004). *jeb[weli]* mutants lack visceral muscle founder cells (Stute et al., 2004), and the small chromosomal deficiency, Df(2R)BSC699 uncovers *jeb*. *hlh54f[delta598]* mutants lack caudal visceral mesoderm.

Sex Identification and Genotyping

Gonad sex identification was accomplished as described by Anllo and colleagues (Anllo et al., 2019). We used Vasa antibody staining to identify larger male gonads, and male specific SGPs (msSGPs). Vasa antibody labels both germ cells and msSGPs, and we identified msSGPs using Vasa antibody alongside a DNA stain to

indicate small, Vasa positive nuclei. Sibling controls were distinguished from homozygous mutants by using fluorescent balancer chromosomes (TM3, P{w[+mC]=Gal4-twi.G}2.3, P{UAS-2xEGFP} AH2.3, Sb[1], Ser[1], FBst0006663; TM6, P{Dfd-EYFP}, Sb, Hu, e; or CyO, P{Dfd-EYFP}).

METHOD DETAILS

Embryonic gonad dissection and Immunostaining

Dissections and immunostaining were performed as previously described (Anllo et al., 2019). Embryos were collected and aged 22-25 hours in a humidified chamber at 25 degrees C for late stage 17 embryos. For younger embryos still undergoing late stages of niche assembly, embryos were aged 22.5-24.5 hours at 23 degrees C. Primary antibodies were used overnight at 4 degrees C. Secondary antibodies were used at 3.75 ug/mL (Alexa488, Cy3, or Alexa647; Molecular Probes; Jackson ImmunoResearch) for 1-2 hr at room temperature. DNA was stained with Hoechst 33342 (Sigma) at 0.2 ug/mL for 5 min.

We used rabbit antibody against Vasa 1:5000 (gift from R. Lehmann, NYU), and RFP 1:500 (Abcam, ab62341); goat antibody against Vasa 1:200 (Santa Cruz, dC-13, now discontinued); mouse antibody against Fasciclin III 1:50 (DSHB, 7G10), Islet 1.5:100 (DSHB 40.3A4; *Drosophila* Tailup), and Gamma Tubulin 1:200 (Sigma, GTU-88); rat antibody against DE-cadherin 1:20 (DSHB, DCAD2); guinea pig antibody against Traffic jam 1:10,000 (gift from D. Godt); and chick antibody against GFP 1:1000 (Aves Labs, GFP-1020). Images of fixed samples were acquired on a Zeiss Imager with Apotome using a 40x, 1.2 N.A. lens or a 20x, 0.8 N.A. lens; or on a Zeiss LSM 880 Confocal with Airyscan and Fast Airyscan, 40x, 1.2 N.A. lens.

in vivo live imaging

Live imaging was performed as previously described (Anllo et al., 2019; Ong et al., 2019). Images were acquired with a Leica DM16000 B spinning disk confocal with a 63 x 1.2 N.A. water immersion objective, using an EMCCD camera (Andor iXon 3 897E or Hamamatsu photonics, model C9100-13) controlled by Metamorph software. Z stacks were taken at 5-minute intervals, with 36 1 um z-slices through the gonad.

Slit and FGF ligand overexpression

The *twi*-Gal4 driver was use to over-express either UAS-*sli.D* or UAS-*ths289.22* in all mesodermal cells. Embryos were collected for 2-3 hours at 29 degrees C, and were aged 15-18 hours at 29 degrees prior to dissection. Just prior to dissection, UAS-eGFP expression was used to distinguish and sort embryos that carried the *twi*-Gal4 driver from sibling controls.

EdU Pulse experiments

EdU pulse experiments were performed using the Click-iT EdU Plus kit (Molecular Probes, c10640) (Salic and Mitchison, 2008). Immediately after dissection, tissue was incubated in 10 uM EdU in *Drosophila* Ringers solution for 30 minutes at room temperature. Tissue was then fixed for 15 min in 4% PFA at room temperature. The azide reaction to couple EdU to alexa647 was performed either prior to, or after antibody staining. Copper catalyst was used at a concentration of 4 nM.

QUANTIFICATION AND STATISTICAL ANALYSIS

Counting niche cells

Niche cells were identified using the niche-cell specific Fasciclin III immunostain. Niche cell nuclei were counted, using either Hoechst DNA stain, or Traffic Jam nuclear stain, as a marker. The ImageJ Cell Counter plugin was used to record counted niche cells. A Mann-Whitney test was used to determine significance of $p < 0.05$.

Quantification of *islet* expression in *slit* and *fgf* mutants

To quantify *islet* expression in Vm ligand mutants, we stained gonads with Islet antibody and used ImageJ to measure the mean gray value fluorescence intensity within regions of interest (ROIs). We selected ROIs including a circular region within somatic cell nuclear boundaries, using Hoechst stain as a marker. For each gonad, 3 niche cell ROIs were measured for Islet expression. An ROI devoid of tissue was selected in a region adjacent to the gonad to determine background fluorescence. Background fluorescence was subtracted from measured niche cell values. Each background-subtracted value was normalized to the mean Islet fluorescence for the gonad, measured at a Z slice including the niche. Mann-Whitney tests were used to determine significance of $p < 0.05$.

Quantification of *islet* expression in *biniou* mutants

To quantify *islet* expression in *biniou* mutants, we stained gonads with Islet antibody and used ImageJ to measure the mean gray value fluorescence intensity within regions of interest (ROIs). We selected ROIs including a circular region within somatic cell nuclear boundaries, using *six4*nlsGFP as a marker. ROIs were in a single Z plane in which the relevant nucleus was in focus. For each gonad, 3 niche cells and 3 non-niche SGP ROIs were measured for Cy3 Islet and for GFP nuclear marker fluorescence. An ROI selected to encompass the unlabeled region of a single germ cell within each gonad was used to determine background fluorescence. Background fluorescence was subtracted from measured values.

To control for possible bleed-through of GFP nuclear marker into the Cy3 Islet channel, we first measured the amount of Cy3 signal that could be accounted for by GFP bleed-through. We plotted the ratio of Cy3 to GFP fluorescence intensity in gonads that were not stained with Islet antibody, and thus should not have any Islet Cy3 signal. This plot determined that Cy3 signal resulting from bleed-through averaged 7% of the GFP signal intensity for each ROI. Thus, in addition to background subtraction, we also subtracted 7% of the GFP signal values from Cy3 values to obtain our final measurements of Cy3 Islet signal. These values were plotted. Mann-Whitney tests were used to determine significance of $p < 0.05$.

Quantification of normalized F actin and E-cadherin fluorescence

To visualize F actin we imaged gonads expressing a GFP-labeled F actin binding protein in the somatic cells, *six4*-eGFP::moesin (Sano et al., 2012). E-cadherin was visualized by immunostaining with an antibody against E-cadherin (DSHB). For all experiments, gonads were dissected and immunostained either with an antibody against GFP, or E-cadherin. Niche interfaces were identified with a Fas3 immunostain. F actin or E-cadherin fluorescence intensity at niche-niche and niche-GSC interfaces was quantified using ImageJ to trace interfaces, and report mean gray values. Background fluorescence was measured as the mean gray value of a line traced where no tissue was present for E-cadherin experiments, or within a germ cell for F actin, as germ cells do not express *six4*-eGFP::moesin. After background subtraction, fluorescence intensity was normalized

by taking the ratio of each interface measurement to the average of all interfaces within that gonad. Normalized values were then plotted, and data was analyzed using a Mann-Whitney test.

Centrosome position quantification

Centrosome position was visualized with immunofluorescence against Gamma tubulin to label pericentriolar material. GSCs were scored for centrosome position if they had already undergone centrosome duplication. We quantified how often one of the two centrosomes was located closer to the adjacent niche than to other neighboring cells. Those GSCs with a centrosome located near the niche-GSC interface were scored as appropriately positioned. GSCs in Vm mutants often failed to maintain a centrosome near the niche. GSCs in Vm mutants that made contact with niche cells at multiple points around their periphery were scored as normal if a centrosome was close to one of these niche-GSC contacts. Data was analyzed using Fisher's exact test.

Quantification of Stat accumulation

To quantify Stat accumulation, we stained gonads with Stat antibody (E. Bach, 1:1000) and used ImageJ to measure the mean gray value fluorescence intensity within regions of interest (ROIs). We selected ROIs including a circular region to sample germ cells, using Vasa immunofluorescence as a marker to delineate cell boundaries. For each gonad, we sampled 5 GSCs and 3 neighboring germ cells. After background subtraction, we measured the ratio of Stat accumulation within each GSC relative to the neighboring germ cell average for that gonad. Relative Stat enrichment values were plotted for each GSC. Mann-Whitney tests were used to evaluate comparisons.

References

Aboim, A. N. (1945). Developpement embryonnair et postembryonnair des gonads normale et agametiques de Drosophila melanogaster. *Rev Suisse Zool* **53**, 53–154.

Anllo, L., Plasschaert, L. W., Sui, J. and DiNardo, S. (2019). Live imaging reveals hub cell assembly and compaction dynamics during morphogenesis of the Drosophila testis niche. *Dev. Biol.* **446**, 102–118.

Azpiazu, N. and Frasch, M. (1993). Tinman and bagpipe: Two homeo box genes that determine cell fates in the dorsal mesoderm of Drosophila. *Genes Dev.* **7**, 1325–1340.

Bataillé, L., Colombié, N., Pelletier, A., Paululat, A., Lebreton, G., Carrier, Y., Frendo, J.-L. and Vincent, A. (2020). Alary muscles and TARMs, a novel type of striated muscles maintaining internal organs positions. *Development* dev.185645.

Battye, R., Stevens, A., Perry, R. L. and Jacobs, J. R. (2001). Repellent signaling by slit requires the leucine-rich repeats. *J. Neurosci.* **21**, 4290–4298.

Blockus, H. and Chédotal, A. (2016). Slit-robo signaling. *Dev.* **143**, 3037–3044.

Boukhatmi, H., Schaub, C., Bataille, L., Reim, I., Frendo, J., Frasch, M. and Vincent, A. (2014). An Org-1 – Tup transcriptional cascade reveals different types of alary muscles connecting internal organs in Drosophila.

Bradley, P. L., Myat, M. M., Comeaux, C. A. and Andrew, D. J. (2003). Posterior migration of the salivary gland requires an intact visceral mesoderm and integrin function. *Dev. Biol.* **257**, 249–262.

Chen, C., Cummings, R., Mordovanakis, A., Hunt, A. J., Mayer, M., Sept, D. and Yamashita, Y. M. (2018). Cytokine receptor-EB1 interaction couples cell polarity and fate during asymmetric cell division. *Elife* **7**, 1–19.

Cimbora, D. M. and Sakonju, S. (1995). Drosophila midgut morphogenesis requires the function of the segmentation gene odd-paired. *Dev. Biol.* **169**, 580–595.

Clark, I. B. N., Muha, V., Klingseisen, A., Leptin, M. and Müller, H. A. J. (2011). Fibroblast growth factor signalling controls successive cell behaviours during mesoderm layer formation in Drosophila. *Development* **138**, 2705–2715.

DeFalco, T. J., Verney, G., Jenkins, A. B., McCaffery, J. M., Russell, S. and Van Doren, M. (2003). Sex-specific apoptosis regulates sexual dimorphism in the Drosophila embryonic gonad. *Dev. Cell* **5**, 205–216.

DeFalco, T., Camara, N., Le Bras, S. and Van Doren, M. (2008). Nonautonomous Sex Determination Controls Sexually Dimorphic Development of the Drosophila Gonad. *Dev. Cell* **14**, 275–286.

Duchek, P., Somogyi, K., Jékely, G., Beccari, S. and Rorth, P. (2001). Guidance of cell migration by the Drosophila PDGF/VEGF receptor. *Cell* **107**, 17–26.

Etienne-Manneville, S. (2008). Polarity proteins in migration and invasion. *Oncogene* **27**, 6970–6980.

Friedl, P. and Gilmour, D. (2009). Collective cell migration in morphogenesis, regeneration and cancer. *Nat. Rev. Mol. Cell Biol.* **10**, 445–457.

Fuller, M. T. (1993). Spermatogenesis. In *The Development of Drosophila melanogaster* (ed. Bate, M.) and Martinez Arias, A.), p. Cold Spring Harbor Labs Press.

Greenspan, L. J. and Matunis, E. L. (2018). Retinoblastoma Intrinsically Regulates Niche Cell Quiescence, Identity, and Niche Number in the Adult Drosophila Testis. *Cell Rep.* **24**, 3466-3476.e8.

Greicius, G. and Virshup, D. M. (2019). Stromal control of intestinal development and the stem cell niche. *Differentiation* **108**, 8–16.

Hardy, R. W., Tokuyasu, K. T., Lindsley, D. L. and Garavito, M. (1979). The germinal proliferation center in the testis of Drosophila melanogaster. *J. Ultrastruct. Res.* **69**, 180–190.

Immerglück, K., Lawrence, P. A. and Bienz, M. (1990). Induction across germ layers in Drosophila mediated by a genetic cascade. *Cell* **62**, 261–268.

Isaacman-Beck, J., Schneider, V., Franzini-Armstrong, C. and Granato, M. (2015). The lh3 Glycosyltransferase Directs Target-Selective Peripheral Nerve Regeneration. *Neuron* **88**, 691–703.

Jenkins, A. B., Mccaffery, J. M. and Doren, M. Van (2003). Drosophila E-cadherin is essential for proper germ cell-soma interaction during gonad morphogenesis. *Development* **130**, 4417–4426.

Jia, L., Cheng, L. and Raper, J. (2005). Slit/Robo signaling is necessary to confine early neural crest cells to the ventral migratory pathway in the trunk. *Dev. Biol.* **282**, 411–421.

Kadam, S., Ghosh, S. and Stathopoulos, A. (2012). Synchronous and symmetric migration of Drosophila caudal visceral mesoderm cells requires dual input by two FGF ligands. *Development* **139**, 699–708.

Kaestner, K. H. (2019). The Intestinal Stem Cell Niche: A Central Role for Foxl1-Expressing Subepithelial Telocytes. *Cmgh* **8**, 111–117.

Kiger, A. A., Jones, D. L., Schulz, C., Rogers, M. B. and Fuller, M. T. (2001). Stem Cell Self-Renewal

Specified by JAK-STAT Activation in Response to a Support Cell Cue. *Science (80-.).* **294**, 2542–2546.

Kitadate, Y. and Kobayashi, S. (2010). Notch and Egfr signaling act antagonistically to regulate germ-line stem cell niche formation in Drosophila male embryonic gonads. *Proc. from Natl. Acad. Sci.* **107**, 14241–14246.

Kraut, R. and Zinn, K. (2004). Roundabout 2 regulates migration of sensory neurons by signaling in trans. *Curr. Biol.* **14**, 1319–1329.

Le Bras, S. and Van Doren, M. (2006). Development of the male germline stem cell niche in Drosophila. *Dev. Biol.* **294**, 92–103.

Leatherman, J. L. and Dinardo, S. (2010). Germline self-renewal requires cyst stem cells and stat regulates niche adhesion in Drosophila testes. *Nat. Cell Biol.* **12**, 806–811.

Leatherman, J. L. and DiNardo, S. (2008). Zfh-1 controls somatic stem cell self-renewal in the Drosophila testis and nonautonomously influences germline stem cell self-renewal. *Cell Stem Cell* **3**, 44–54.

Lee, S., Zhou, L., Kim, J., Kalbfleisch, S. and Scho, F. (2008). Lasp anchors the Drosophila male stem cell niche and mediates spermatid individualization. *Mech. Dev.* **125**, 768–776.

Losick, V. P., Morris, L. X., Fox, D. T. and Spradling, A. (2011). Drosophila Stem Cell Niches: A Decade of Discovery Suggests a Unified View of Stem Cell Regulation. *Dev. Cell* **21**, 159–171.

Martino, P. A., Heitman, N. and Rendl, M. (2021). The dermal sheath: An emerging component of the hair follicle stem cell niche. *Exp. Dermatol.* **30**, 512–521.

McMahon, A., Reeves, G. T., Supatto, W. and Stathopoulos, A. (2010). Mesoderm migration in Drosophila is a multi-step process requiring FGF signaling and integrin activity. *Development* **137**, 2167–2175.

Montell, D. J. (2003). Border-cell migration: the race is on. *Nat. Rev. Mol. Cell Biol.* **4**, 13–24.

Moore, K. A. and Lemischka, I. R. (2006). Stem cells and their niches. *Science (80-.).* **311**, 1800–1885.

Morrison, S. J. and Spradling, A. C. (2008). Stem Cells and Niches□: Mechanisms That Promote Stem Cell Maintenance throughout Life. *Cell* **132**, 598–611.

Nelson, K. A., Warder, B. N., Dinardo, S. and Anllo, L. (2020). Dissection and live-imaging of the late embryonic drosophila gonad. *J. Vis. Exp.* **2020**, 1–19.

Nusslein-Volhard, C., Wieschaus, E. and Kluding, H. (1984). Mutations affecting the pattern of the larval cuticle in Drosophila melanogaster. *Wilhelm Roux's Arch. Dev. Biol.* **193**, 267–282.

Okegbe, T. C. and DiNardo, S. (2011). The endoderm specifies the mesodermal niche for the germline in Drosophila via Delta-Notch signaling. *Development* **138**, 1259–1267.

Ong, K., Collier, C. and DiNardo, S. (2019). Multiple feedback mechanisms fine-tune Rho signaling to regulate morphogenetic outcomes. *J. Cell Sci.* **132**,.

Papagiannouli, F., Schardt, L., Grajcarek, J., Ha, N. and Lohmann, I. (2014). The Hox Gene Abd-B Controls Stem Cell Niche Function in the Drosophila Testis. *Dev. Cell* **28**, 189–202.

Rompalos, P. and Greco, V. (2014). Stem cell dynamics in the hair follicle niche. *Semin Cell Dev Biol* **0**, 34–42.

Rothberg, J. M., Jacobs, J. R., Goodman, C. S. and Artavanis-Tsakonas, S. (1990). slit: An extracellular protein necessary for development of midline glia and commissural axon pathways contains both EGF and LRR domains. *Genes Dev.* **4**, 2169–2187.

Salic, A. and Mitchison, T. J. (2008). A chemical method for fast and sensitive detection of DNA synthesis in vivo. *Proc. from Natl. Acad. Sci.* **105**, 2415-.

Sandmann, T., Jensen, L. J., Jakobsen, J. S., Karzynski, M. M., Eichenlaub, M. P., Bork, P. and Furlong, E. E. M. (2006). A Temporal Map of Transcription Factor Activity: Mef2 Directly Regulates Target Genes at All Stages of Muscle Development. *Dev. Cell* **10**, 797–807.

Sano, H., Kunwar, P. S., Renault, A. D., Barbosa, V., Clark, I. B. N., Ishihara, S., Sugimura, K. and Lehmann, R. (2012). The Drosophila Actin Regulator ENABLED Regulates Cell Shape and Orientation during Gonad Morphogenesis. *PLoS One* **7**,.

Santiago, C. and Bashaw, J. (2014). Transcription factors and effectors that regulate neuronal morphology. *Dev.* **141**, 4667–4680.

Santiago, C. and Bashaw, G. J. (2017). Islet Coordinately Regulates Motor Axon Guidance and Dendrite Targeting through the Frazzled/DCC Receptor. *Cell Rep.* **18**, 1646–1659.

Scarpa, E. and Mayor, R. (2016). Collective cell migration in development. *J. Cell Biol.* **212**, 143–155.

Sheng, X. R. and Matunis, E. (2011). Live imaging of the Drosophila spermatogonial stem cell niche reveals novel mechanisms regulating germline stem cell output. *Development* **138**, 3367–3376.

Sheng, X. R., Posenau, T., Gumulak-Smith, J. J., Matunis, E., Van Doren, M. and Wawersik, M. (2009). Jak-STAT regulation of male germline stem cell establishment during Drosophila embryogenesis. *Dev.*

Biol. **334**, 335–344.

Shwartz, Y., Gonzalez-Celeiro, M., Chen, C. L., Pasolli, H. A., Sheu, S. H., Fan, S. M. Y., Shamsi, F., Assaad, S., Lin, E. T. Y., Zhang, B., et al. (2020). Cell Types Promoting Goosebumps Form a Niche to Regulate Hair Follicle Stem Cells. *Cell* **182**, 578-593.e19.

Sinden, D., Badgett, M., Fry, J., Jones, T., Palmen, R., Sheng, X., Simmons, A., Matunis, E. and Wawersik, M. (2012). Jak-STAT regulation of cyst stem cell development in the Drosophila testis. *Dev. Biol.* **372**, 5–16.

Soplop, N. H., Cheng, Y. S. and Kramer, S. G. (2012). Roundabout is required in the visceral mesoderm for proper microvillus length in the hindgut epithelium. *Dev. Dyn.* **241**, 759–769.

Stathopoulos, A., Tam, B., Ronshaugen, M., Frasch, M. and Levine, M. (2004). pyramis and thisbe: FGF genes that pattern the mesoderm of Drosophila embryos. *Genes Dev.* **18**, 687–699.

Stute, C., Schimmelpfeng, K., Renkawitz-Pohl, R., Palmer, R. H. and Holz, A. (2004). Myoblast determination in the somatic and visceral mesoderm depends on Notch signalling as well as on milliways (miliAlk) as receptor for jeb signalling. *Development* **131**, 743–754.

Sun, J. and Stathopoulos, A. (2018). Fgf controls epithelial-mesenchymal transitions during gastrulation by regulating cell division and apicobasal polarity. *Dev.* **145**,.

Sutherland, D., Samakovlis, C. and Krasnow, M. A. (1996). branchless encodes a Drosophila FGF homolog that controls tracheal cell migration and the pattern of branching. *Cell* **87**, 1091–1101.

Tanentzapf, G., Devenport, D., Godt, D. and Brown, N. H. (2007). Integrin-dependent anchoring of a stem-cell niche. *Nat. Cell Biol.* **9**, 1413–1418.

Tepass, U. and Hartenstein, V. (1994). Epithelium formation in the Drosophila midgut depends on the interaction of endoderm and mesoderm. *Development* **120**, 579–590.

Tulina, N. and Matunis, E. (2001). Control of Stem Cell Self-Renewal in Drosophila Spermatogenesis by JAK-STAT Signaling. *Science (80-.).* **294**, 2546–2550.

Vassilev, V., Platek, A., Hiver, S., Enomoto, H. and Takeichi, M. (2017). Catenins Steer Cell Migration via Stabilization of Front-Rear Polarity. *Dev. Cell* **43**, 463-479.e5.

Vlodavsky, I., Bar-Shavit, R., Ishar-Michael, R., Bashkin, P. and Fuks, Z. (1991). Extracellular sequestration and release of fibroblast growth factor: a regulatory mechanism? *Trends Biochem. Sci.* **16**,

268–271.

Voog, J., D'Alterio, C. and Jones, D. L. (2008). Multipotent somatic stem cells contribute to the stem cell niche in the Drosophila testis. *Nature* **454**, 1132–1136.

Wang, C., Chen, J., Wen, P., Sun, P. and Xi, R. (2016). Chapter 2: Stem Cell Niche. In *Regenerative Medicine - from Protocol to Patient: 1. Biology of Tissue Regeneration: Third Edition* (ed. Steinhoff, G.), pp. 57–85. Springer International Publishing Switzerland.

Weiss, J. B., Suyama, K. L., Lee, H. H. and Scott, M. P. (2001). Jelly belly: A Drosophila LDL receptor repeat-containing signal required for mesoderm migration and differentiation. *Cell* **107**, 387–398.

Weyers, J. J., Milutinovich Allison B., A. B., Takeda, Y., Jemc, J. C. and Van Doren, M. (2011). A genetic screen for mutations affecting gonad formation in Drosophila reveals a role for the slit/robo pathway. *Dev. Biol.* **353**, 217–228.

Xiao, T., Staub, W., Robles, E., Gosse, N. J., Cole, G. J. and Baier, H. (2011). Assembly of lamina-specific neuronal connections by Slit bound to type IV Collagen. *Cell* **146**, 164–176.

Yamashita, Y. M., Jones, D. L. and Fuller, M. T. (2003). Orientation of asymmetric stem cell division by the APC tumor suppressor and centrosome. *Science (80-.).* **301**, 1547–1550.

Yamashita, Y. M., Mahowald, A. P., Perlin, J. R. and Fuller, M. T. (2007). Asymmetric inheritance of mother versus daughter centrosome in stem cell division. *Science (80-.).* **315**, 518–521.

Zaffran, S., Küchler, A., Lee, H. H. and Frasch, M. (2001). biniou (FoxF), a central component in a regulatory network controlling visceral mesoderm development and midgut morphogenesis in Drosophila. *Genes Dev.* **15**, 2900–2915.

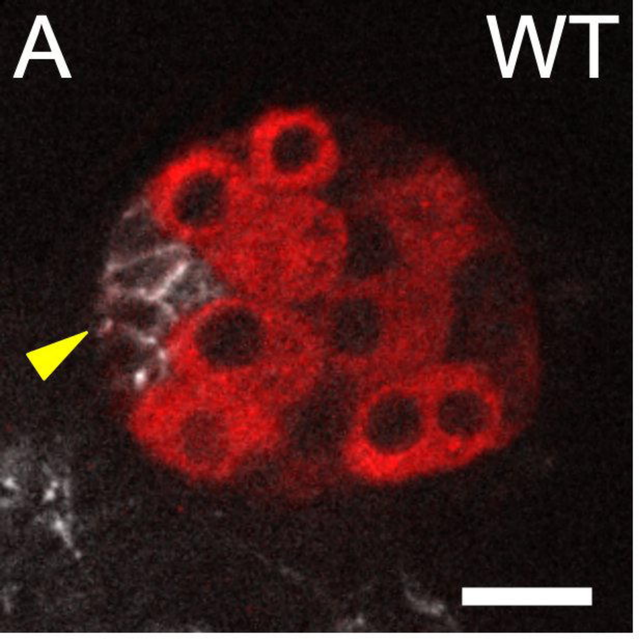

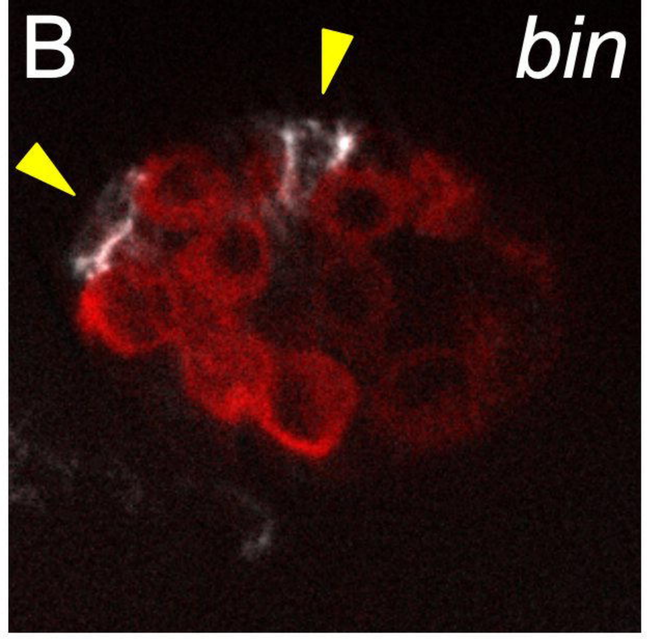

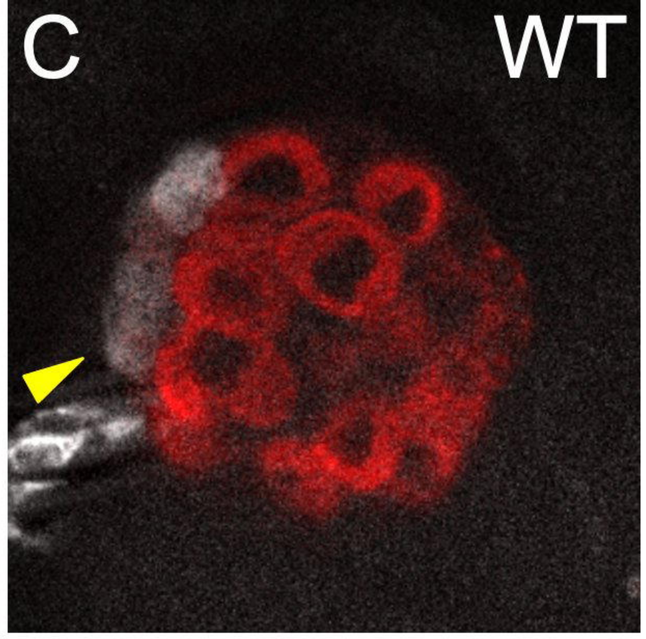

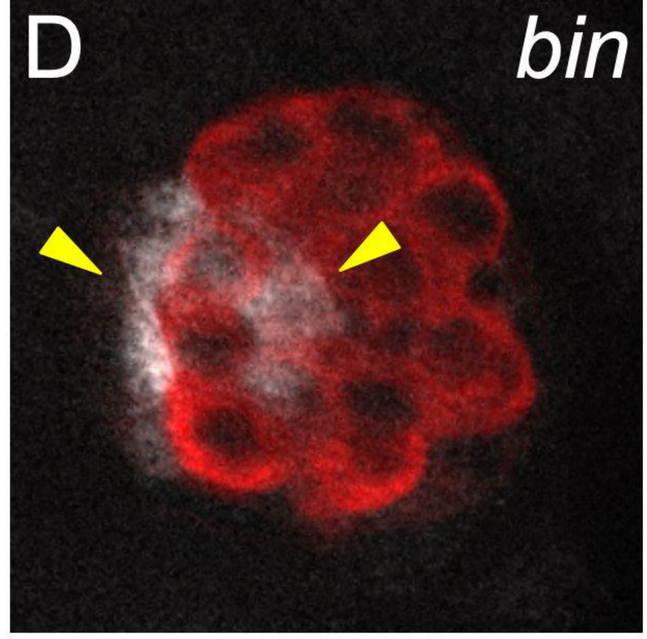

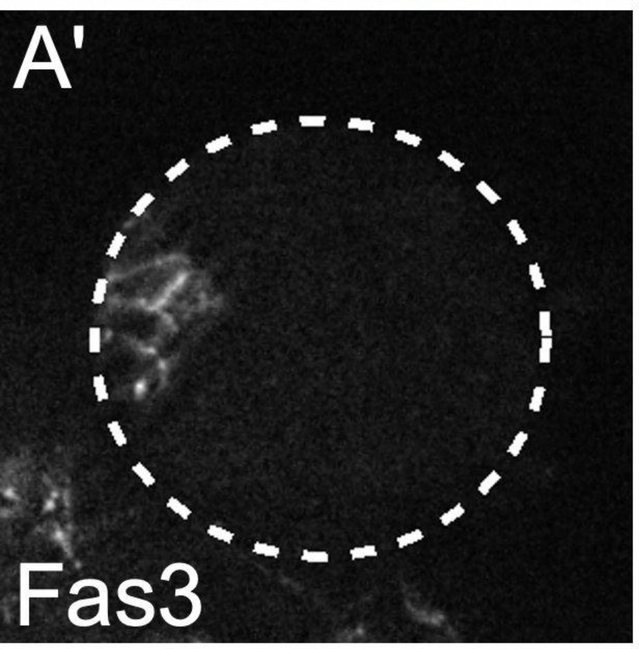

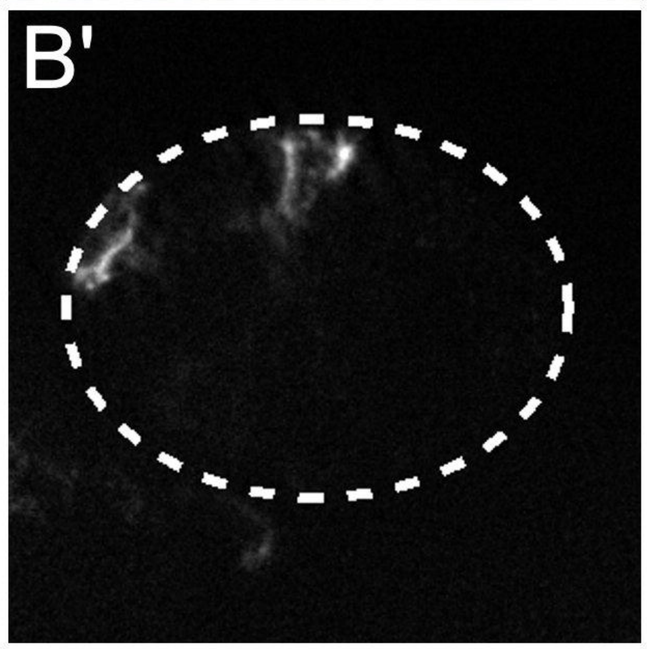

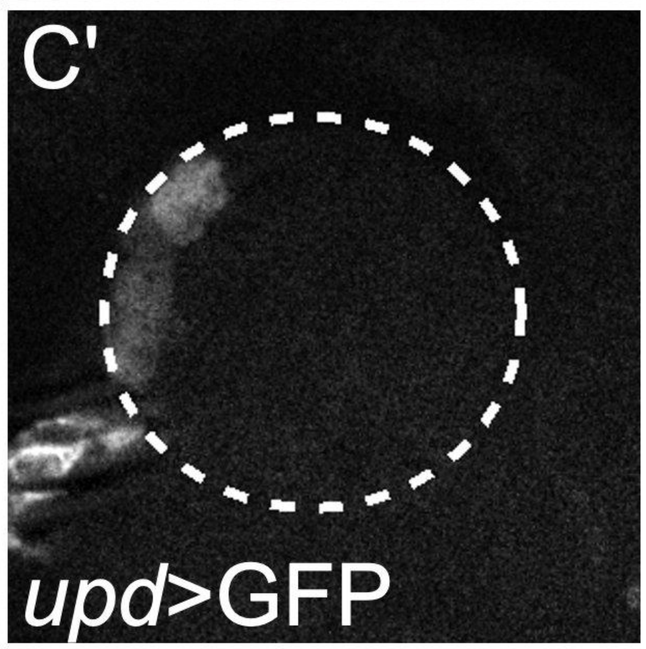

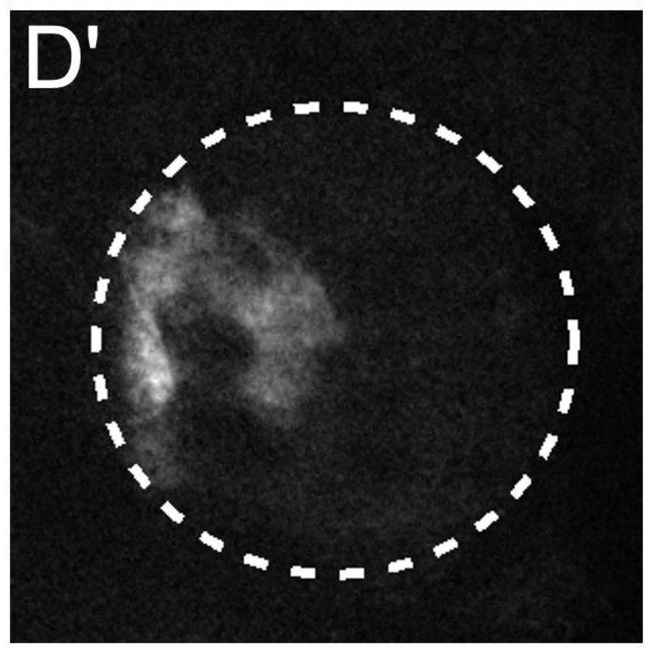

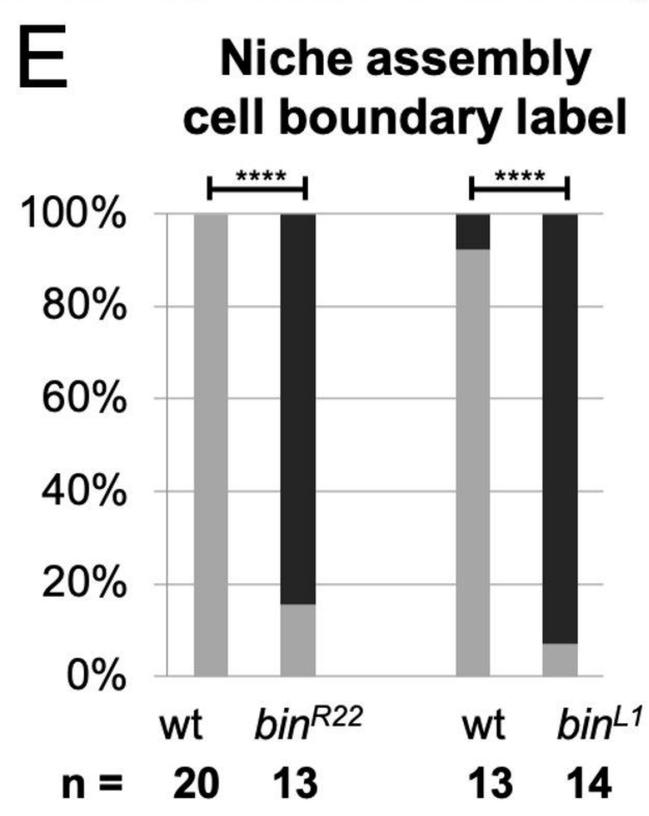

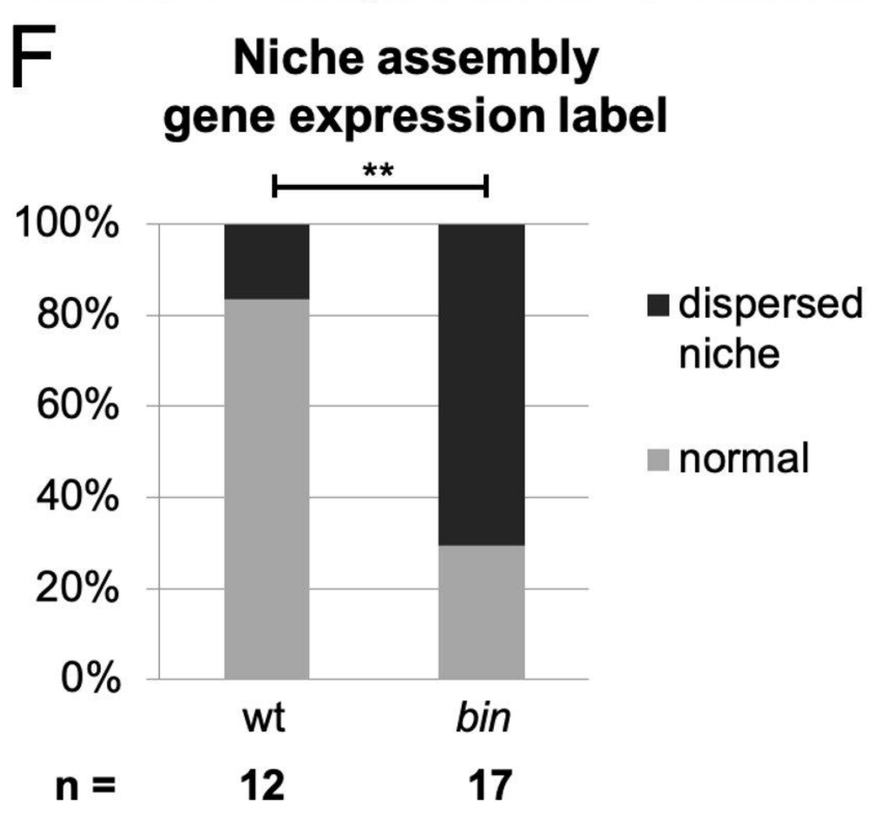

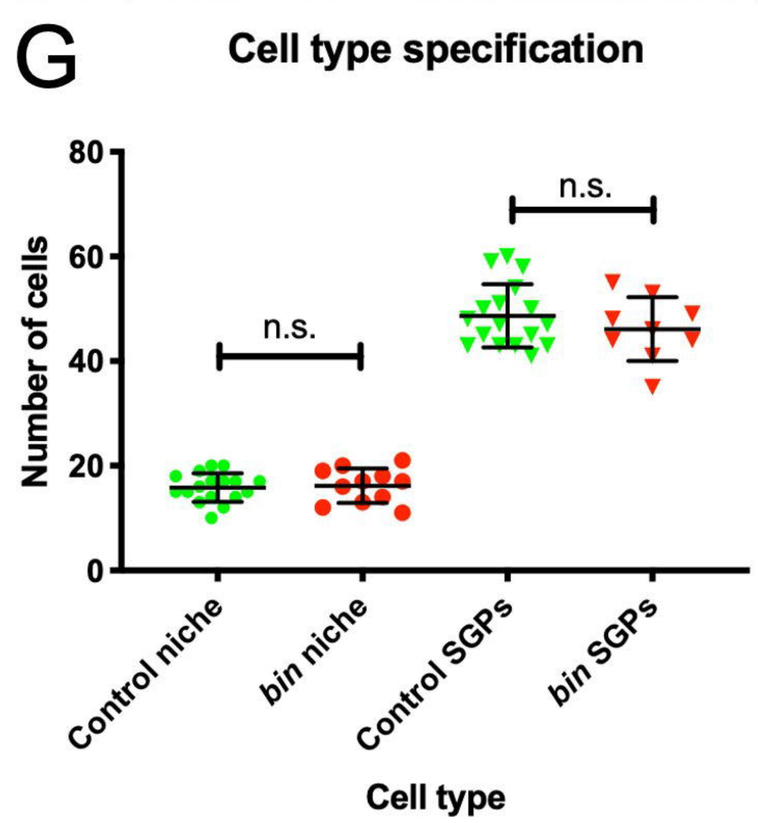

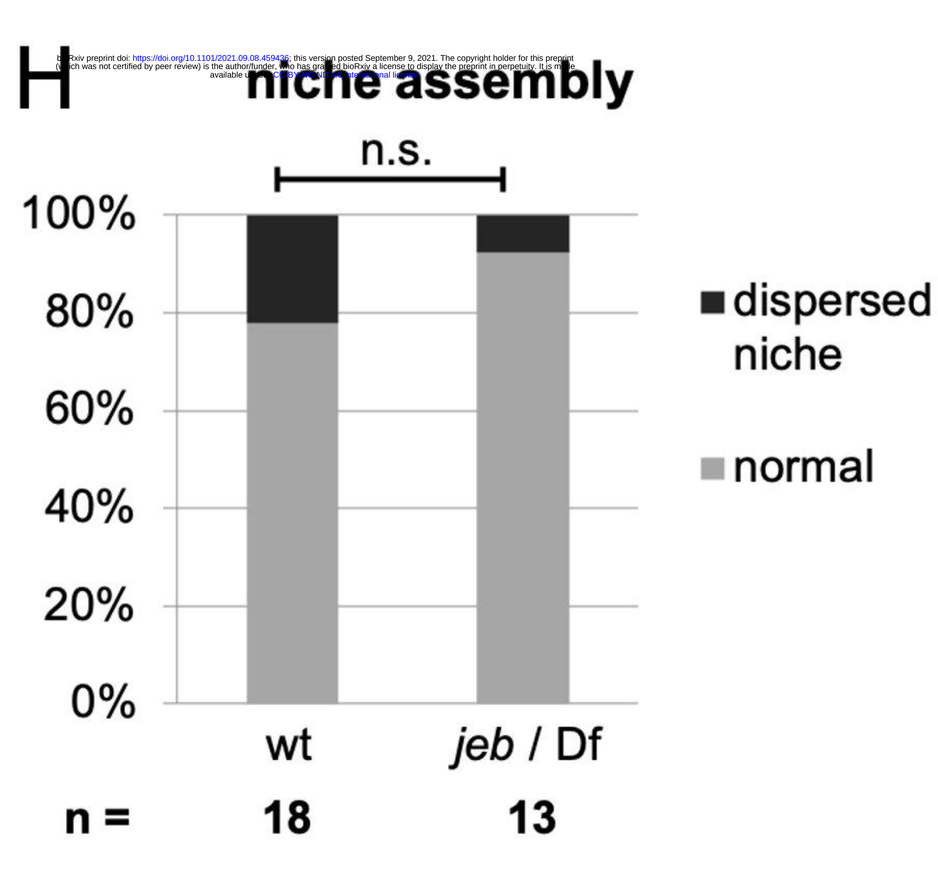

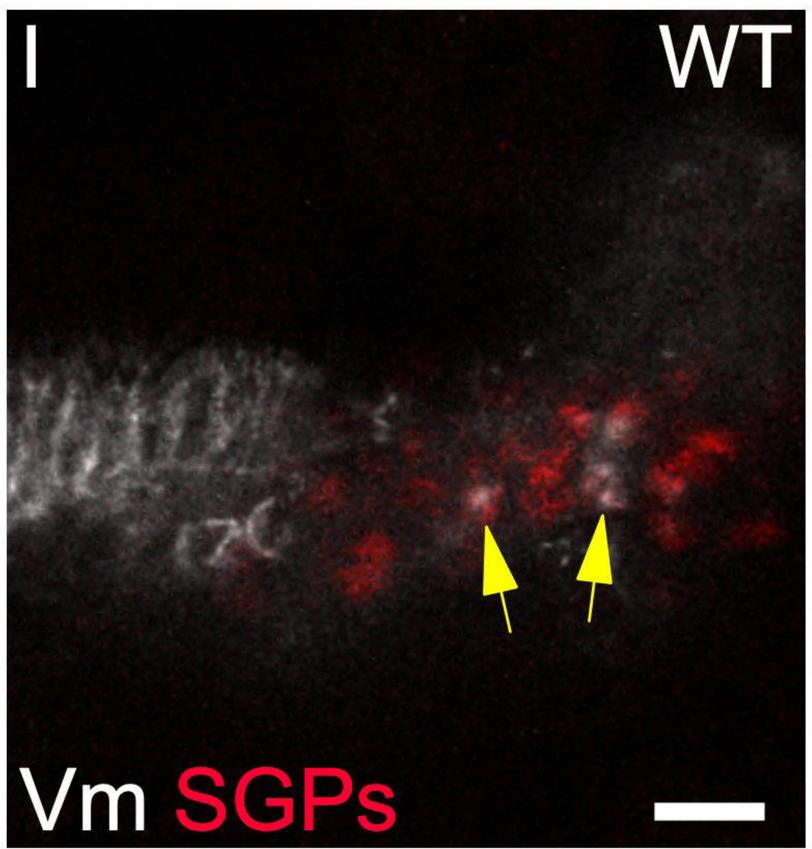

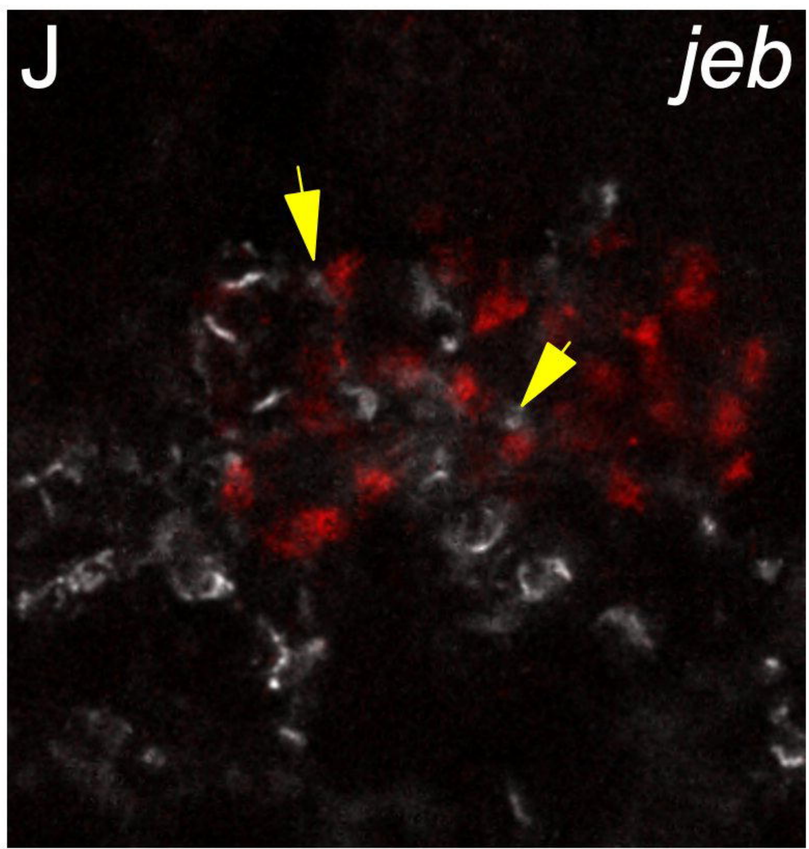

A WT

B *fgf*

C *fgf*

D *slit*

A'

B'

C'

D'

E

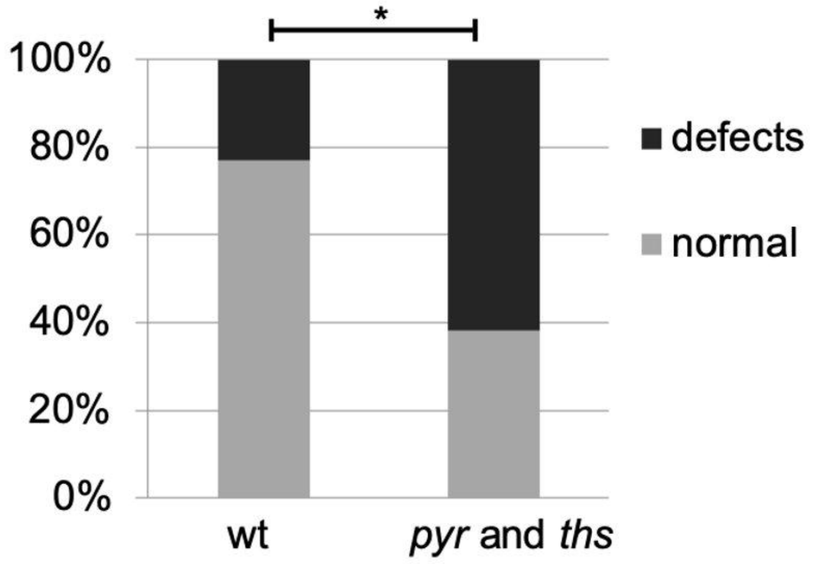

F

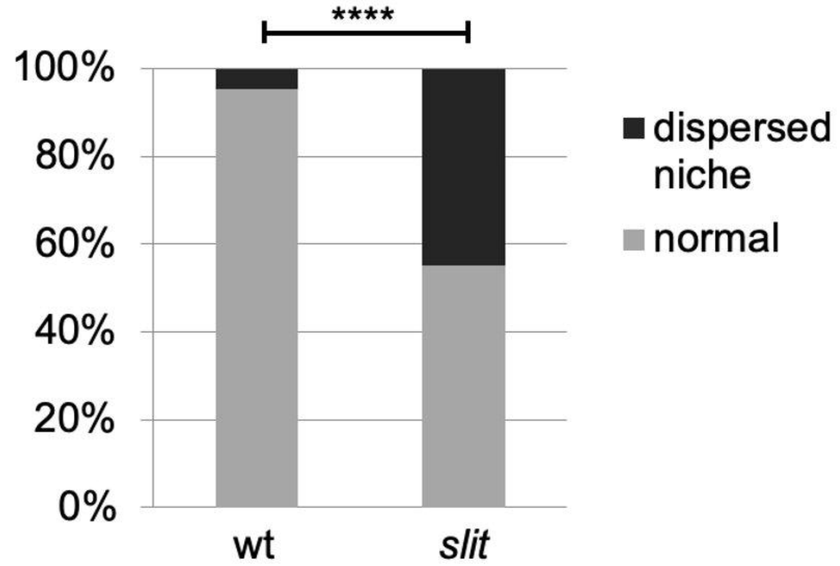

G

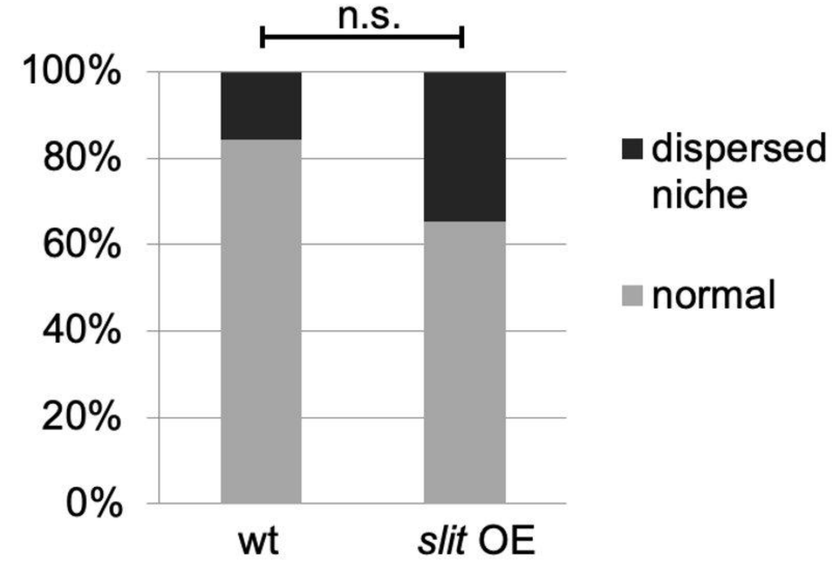

H *fgf* & *slit*

H'

I

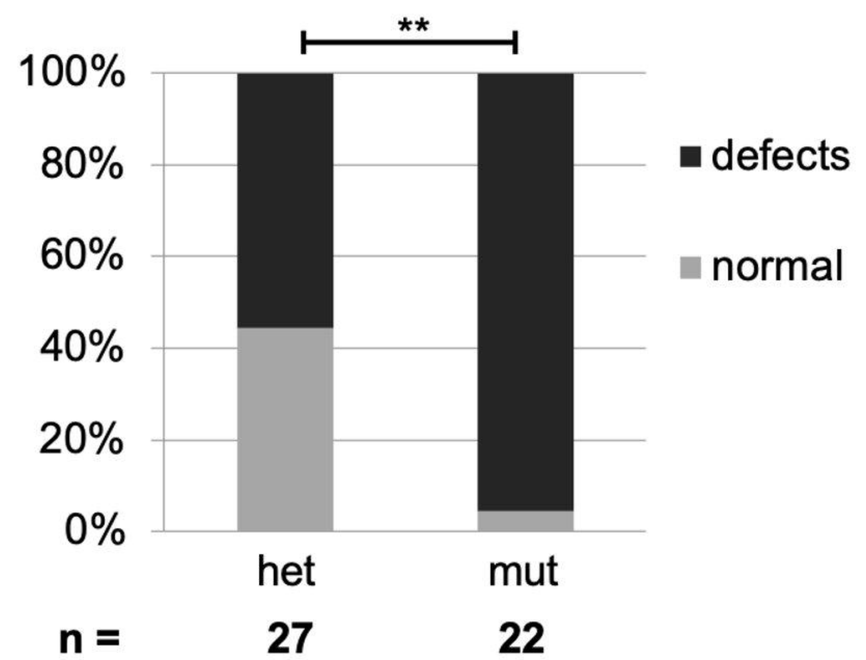

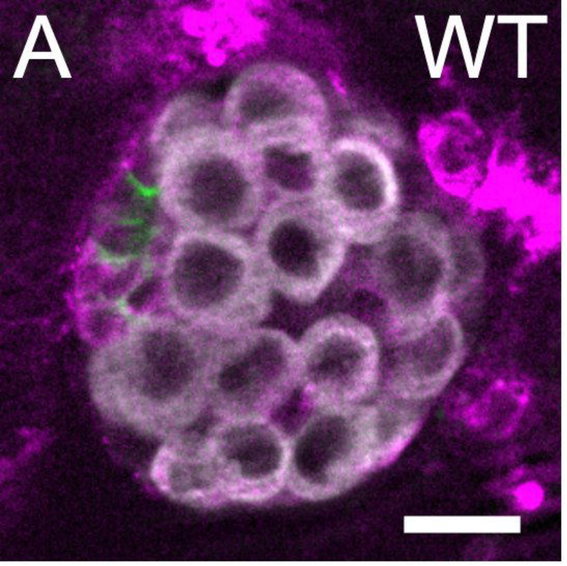
A
WT

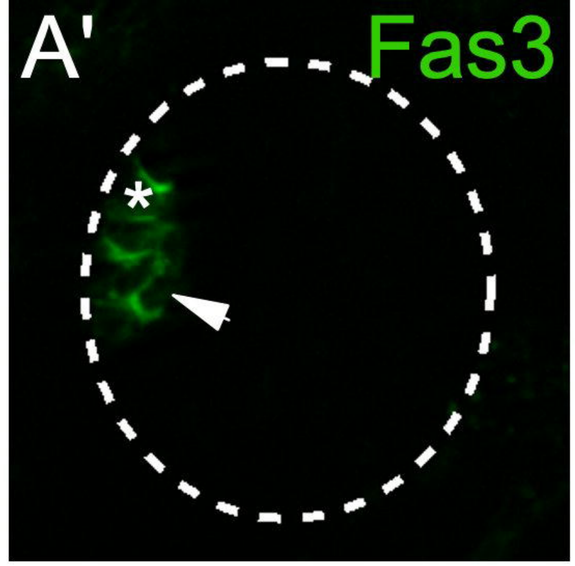
A'
Fas3

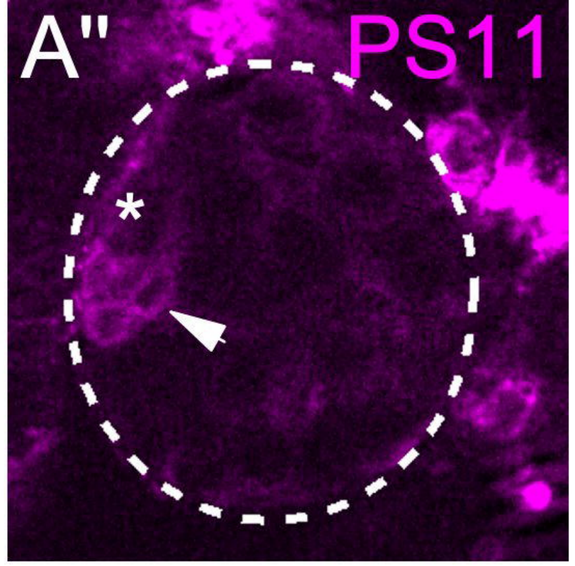
A''
PS11

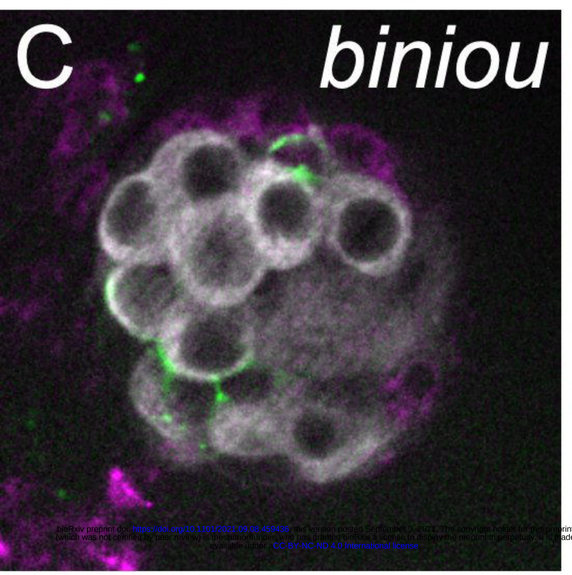
C
biniou

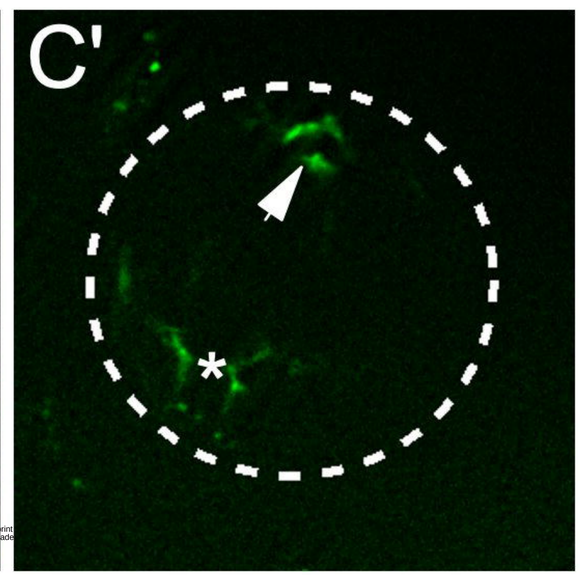
C'

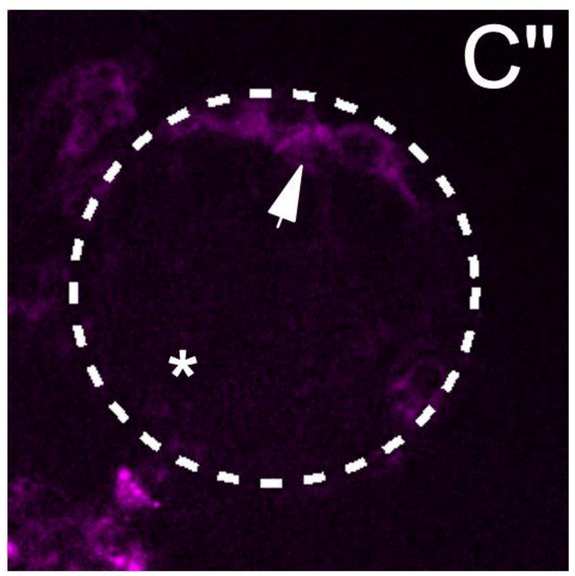
C''

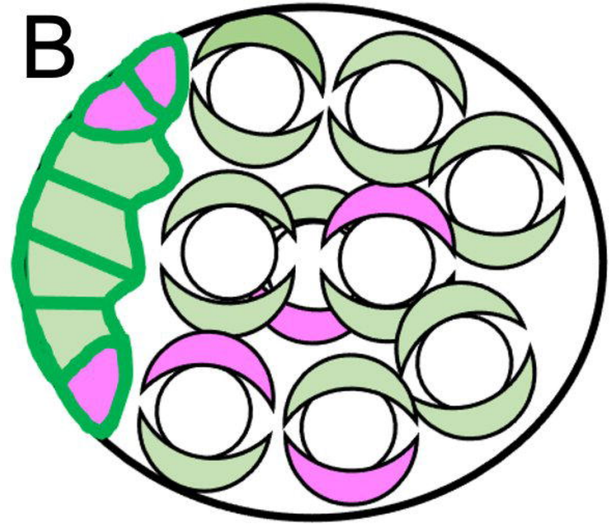
B
germ cell
SGP
PS11 SGP
niche cell

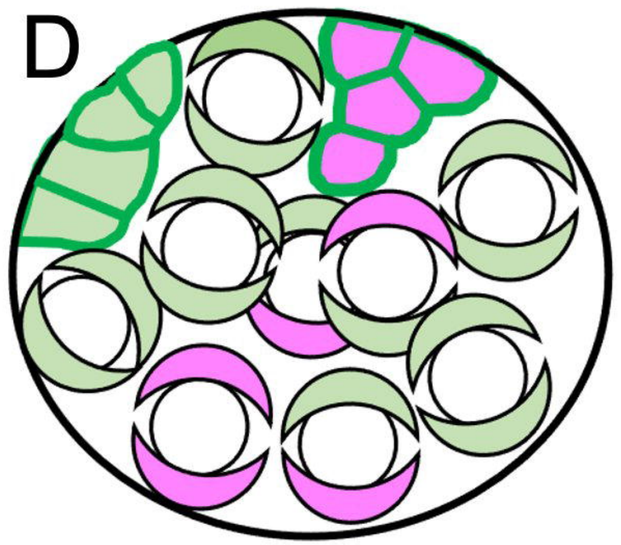
D

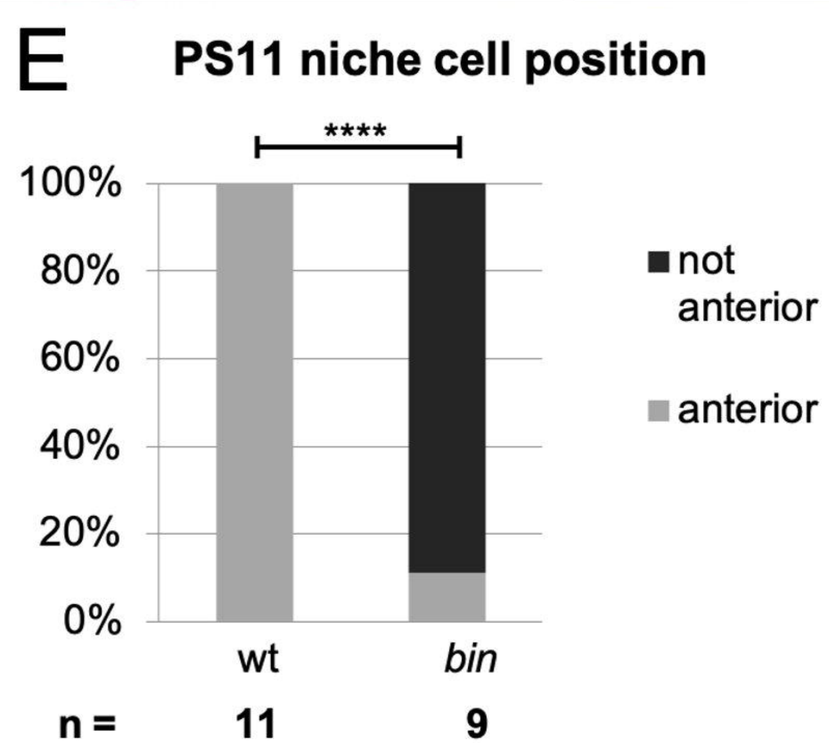
E
PS11 niche cell position
****
100%
80%
60%
40%
20%
0%
wt
bin
n =
11
9
not anterior
anterior

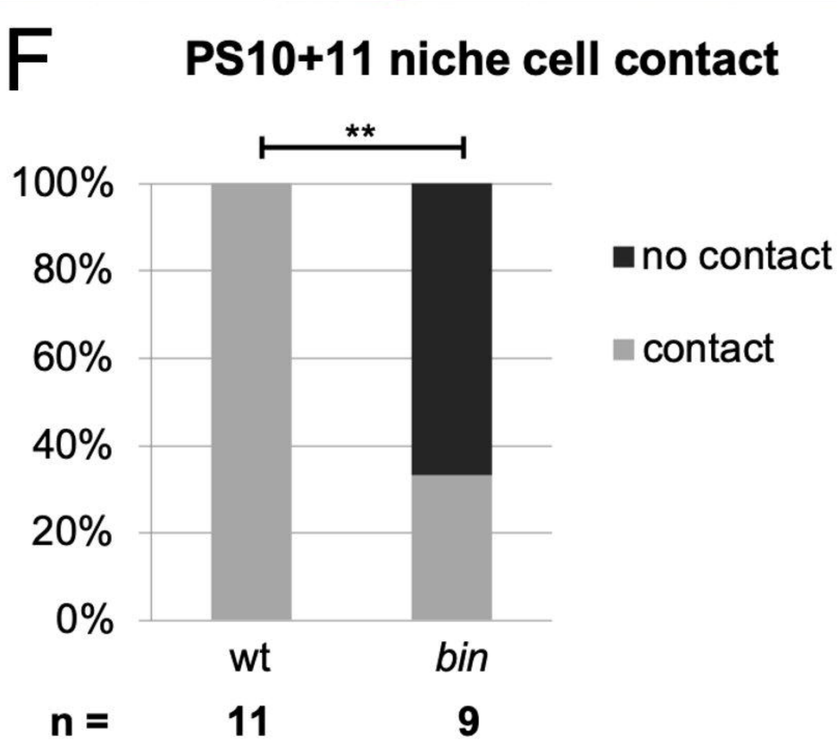
F
PS10+11 niche cell contact
**
100%
80%
60%
40%
20%
0%
wt
bin
n =
11
9
no contact
contact

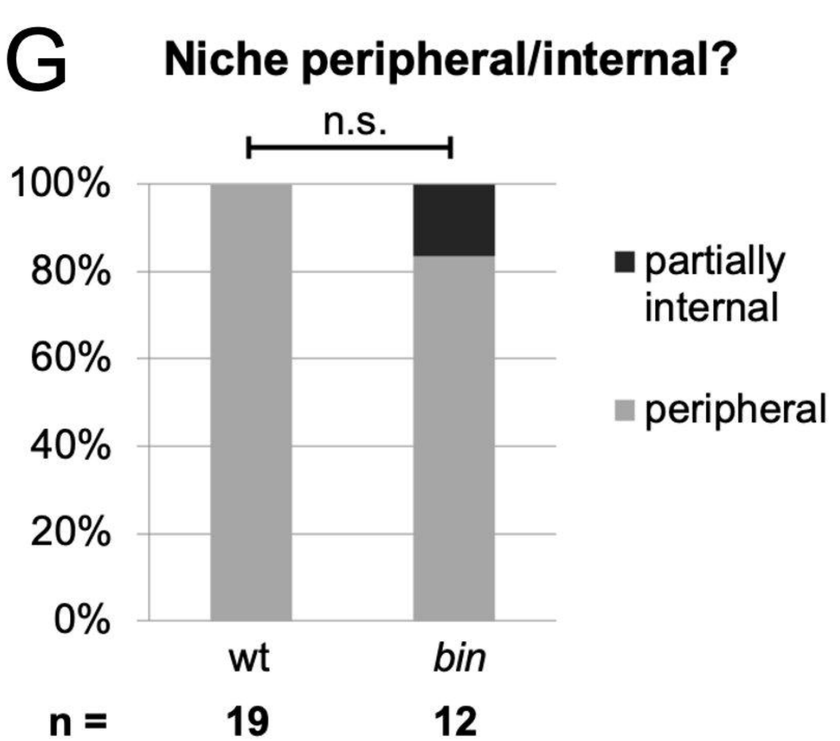
G
Niche peripheral/internal?
n.s.
100%
80%
60%
40%
20%
0%
wt
bin
n =
19
12
partially internal
peripheral

A WT

B Niche F-Actin

normalized fluorescence

****

niche-niche

niche-GSC

Interface

C WT

D Niche E-cad

normalized fluorescence

****

niche-niche

niche-GSC

Interface

E F-Actin during assembly

normalized fluorescence

****

niche-niche

niche-GC

Interface

F F-Actin after assembly

normalized fluorescence

****

niche-niche

niche-GSC

Interface

G 00:00 00:30 00:50

H *bin*

I Niche F-Actin without Vm

normalized fluorescence

n.s.

niche-niche

niche-GSC

Interface

J *bin*

K Niche E-cad without Vm

normalized fluorescence

n.s.

niche-niche

niche-GSC

Interface

L *fgf* E-cad

M *slit*

N E-cad in *fgf* mutants

normalized fluorescence

*

n.s.

* p = 0.016

WT n-n

WT n-g

FGF n-n

FGF n-g

Interface

O E-cad in *slit* mutants

normalized fluorescence

*

n.s.

* p = 0.030

WT n-n

WT n-g

slit n-n

slit n-g

Interface

A WT

A'

A''

Islet

B

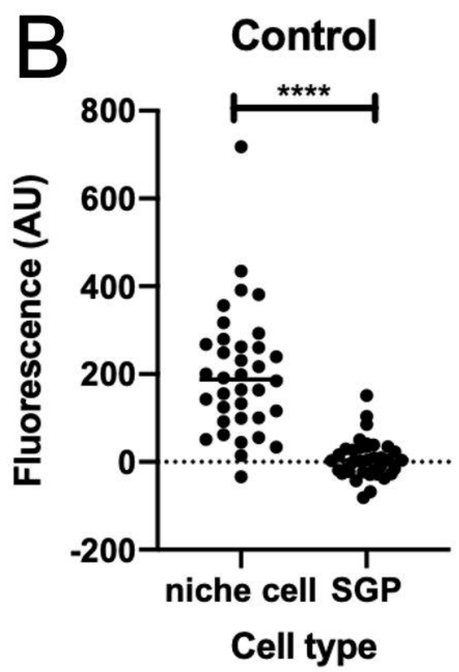

C *biniou*

C'

C''

Islet

D

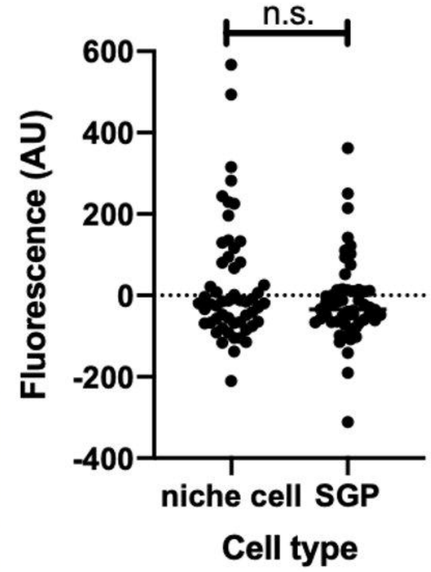

E WT

E'

F *fgf*

F'

Islet niche

Islet niche

G *slit*

G'

Islet niche

H

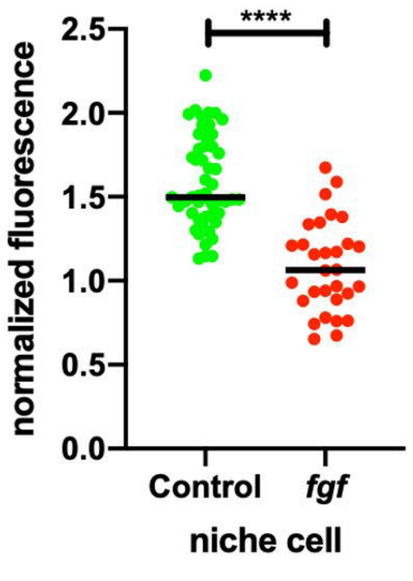

I

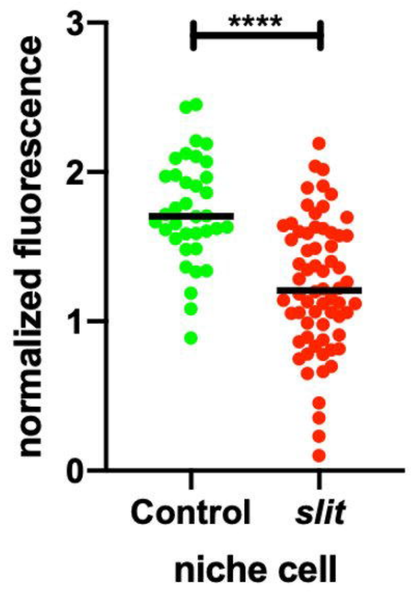

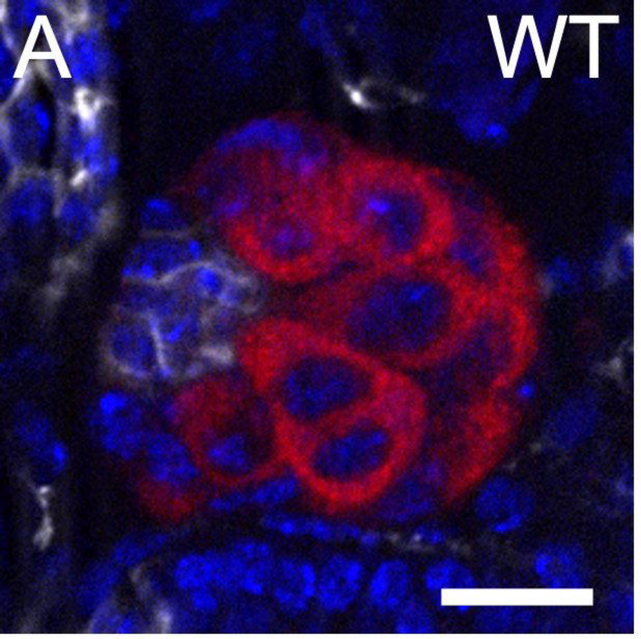

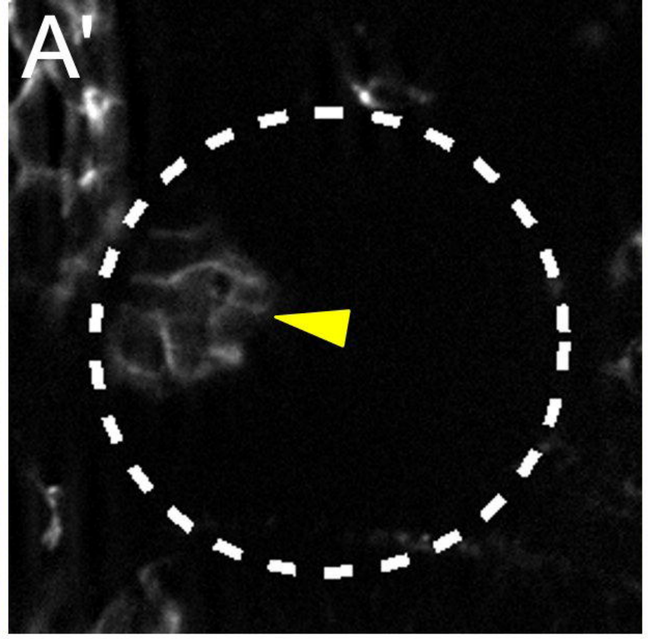

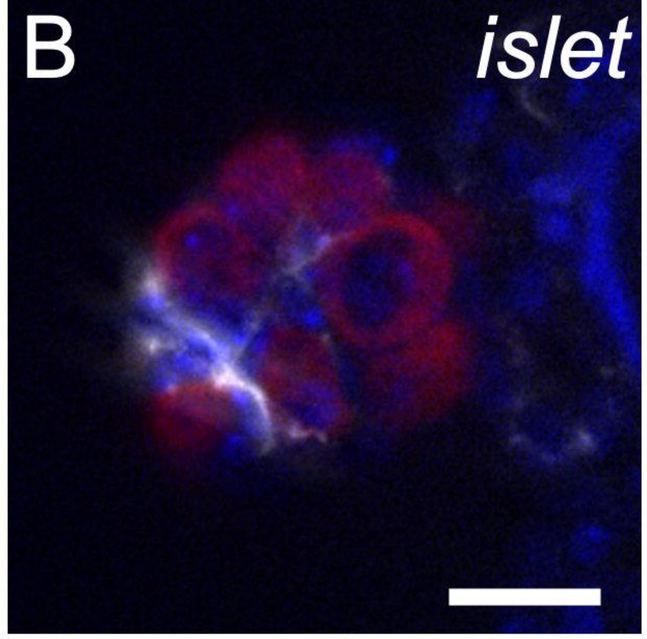

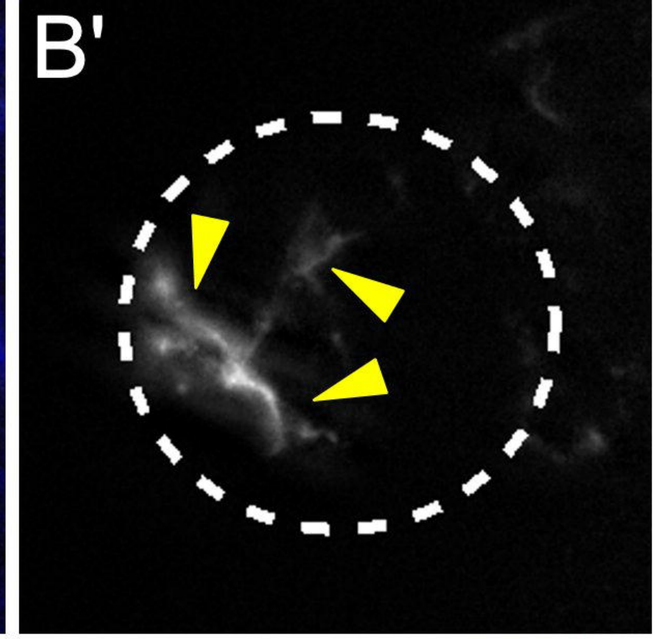

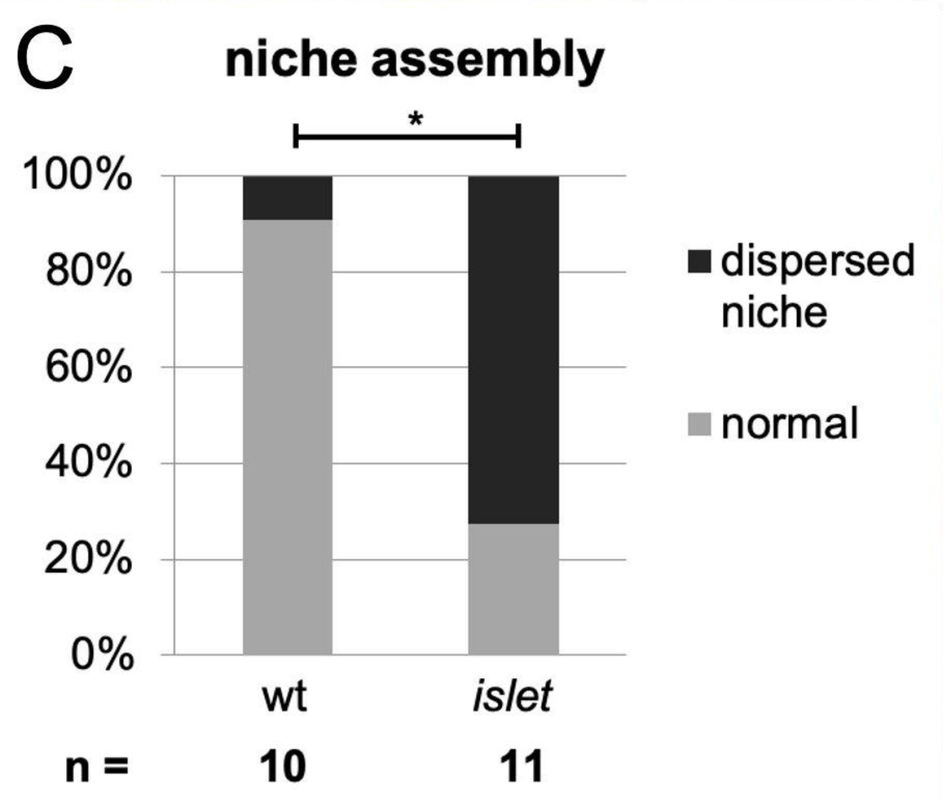

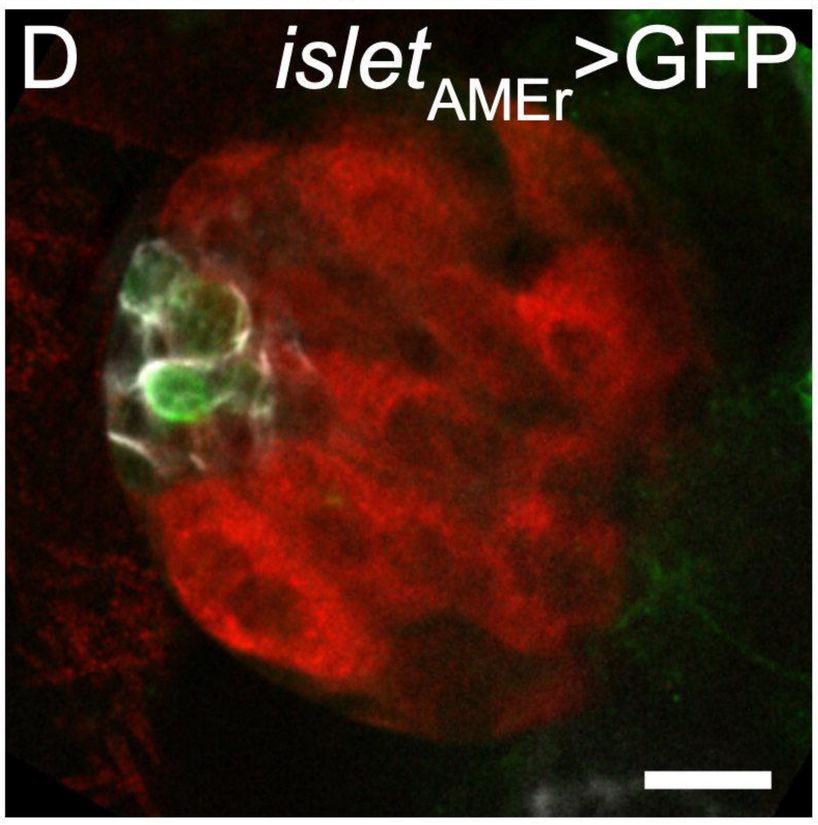

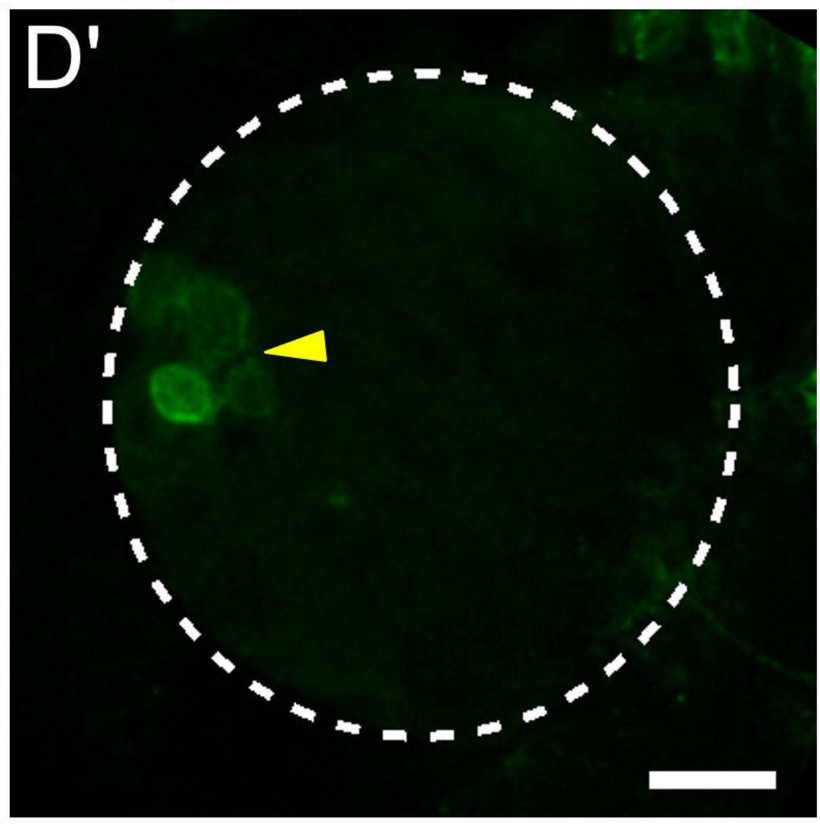

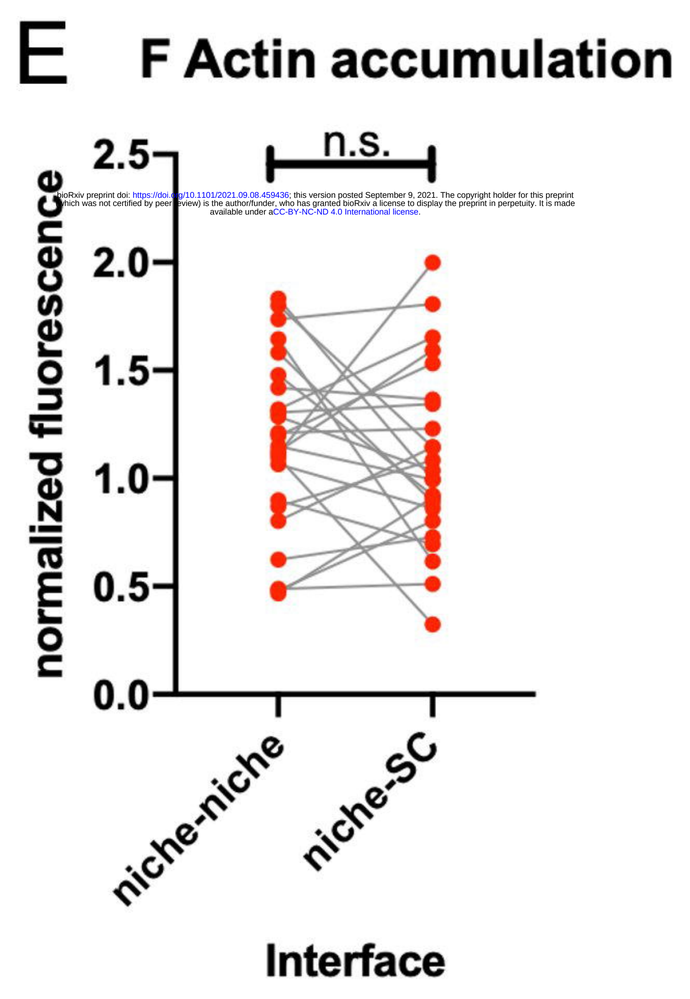

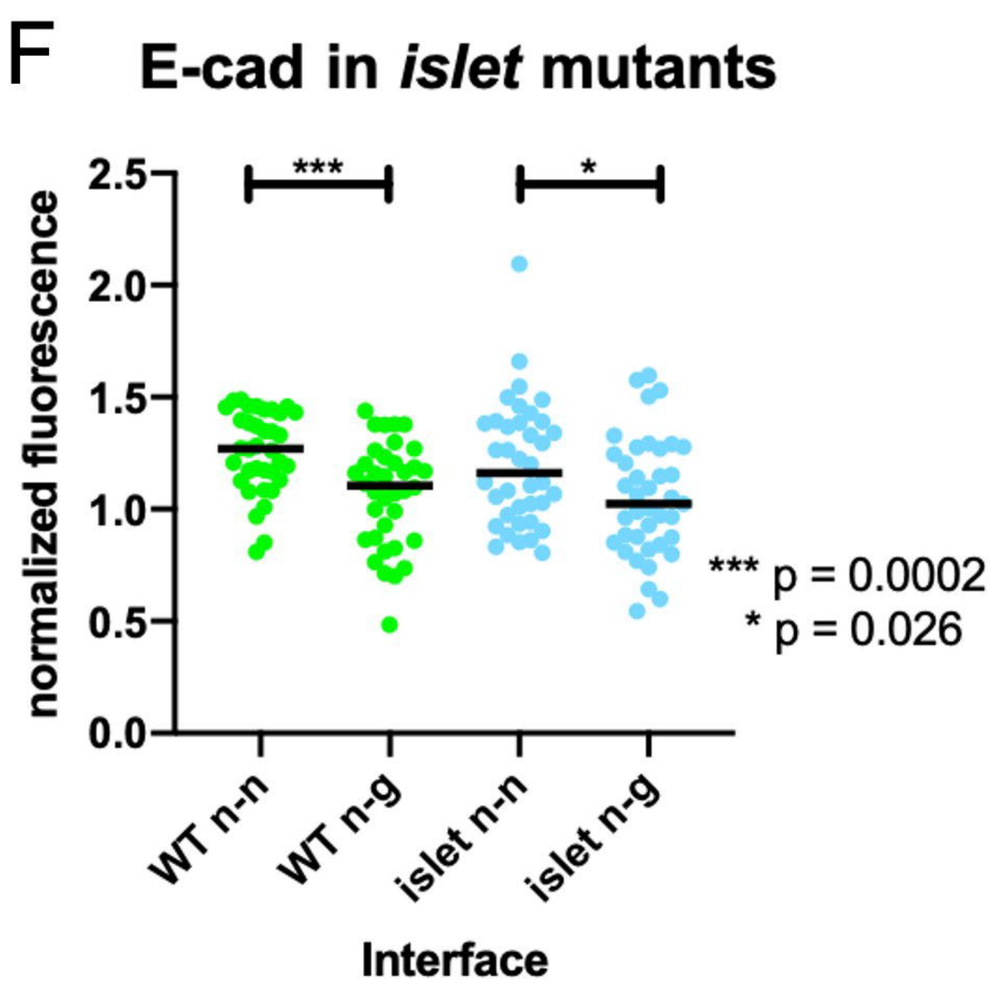

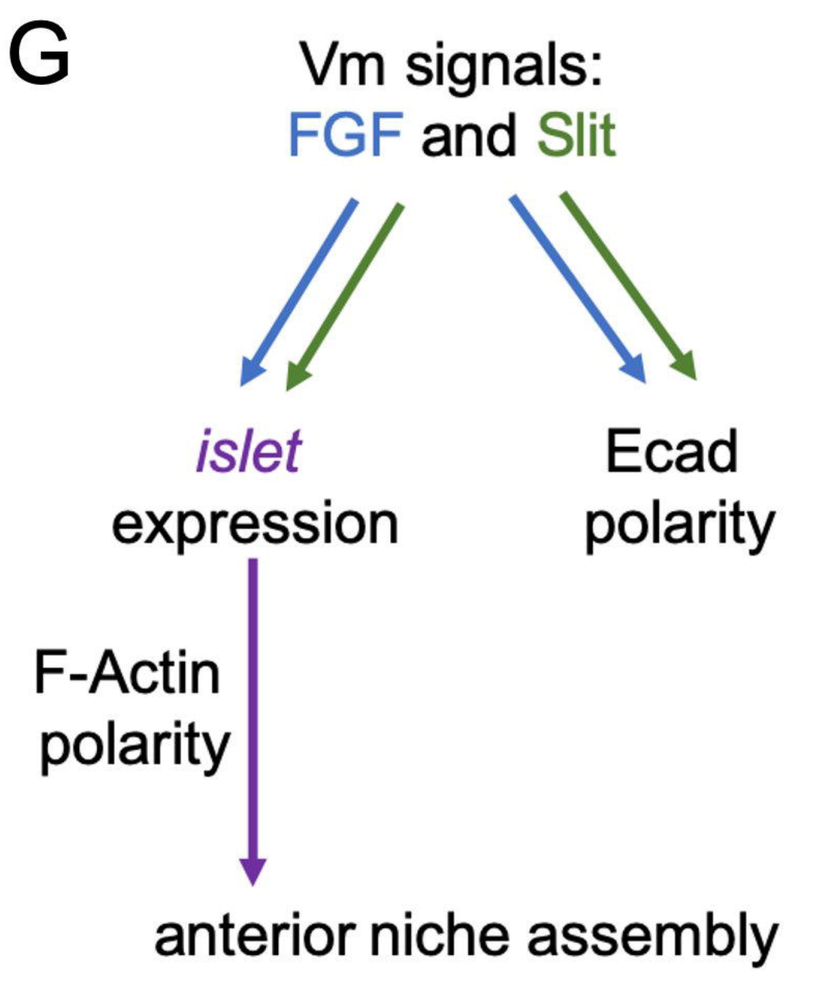

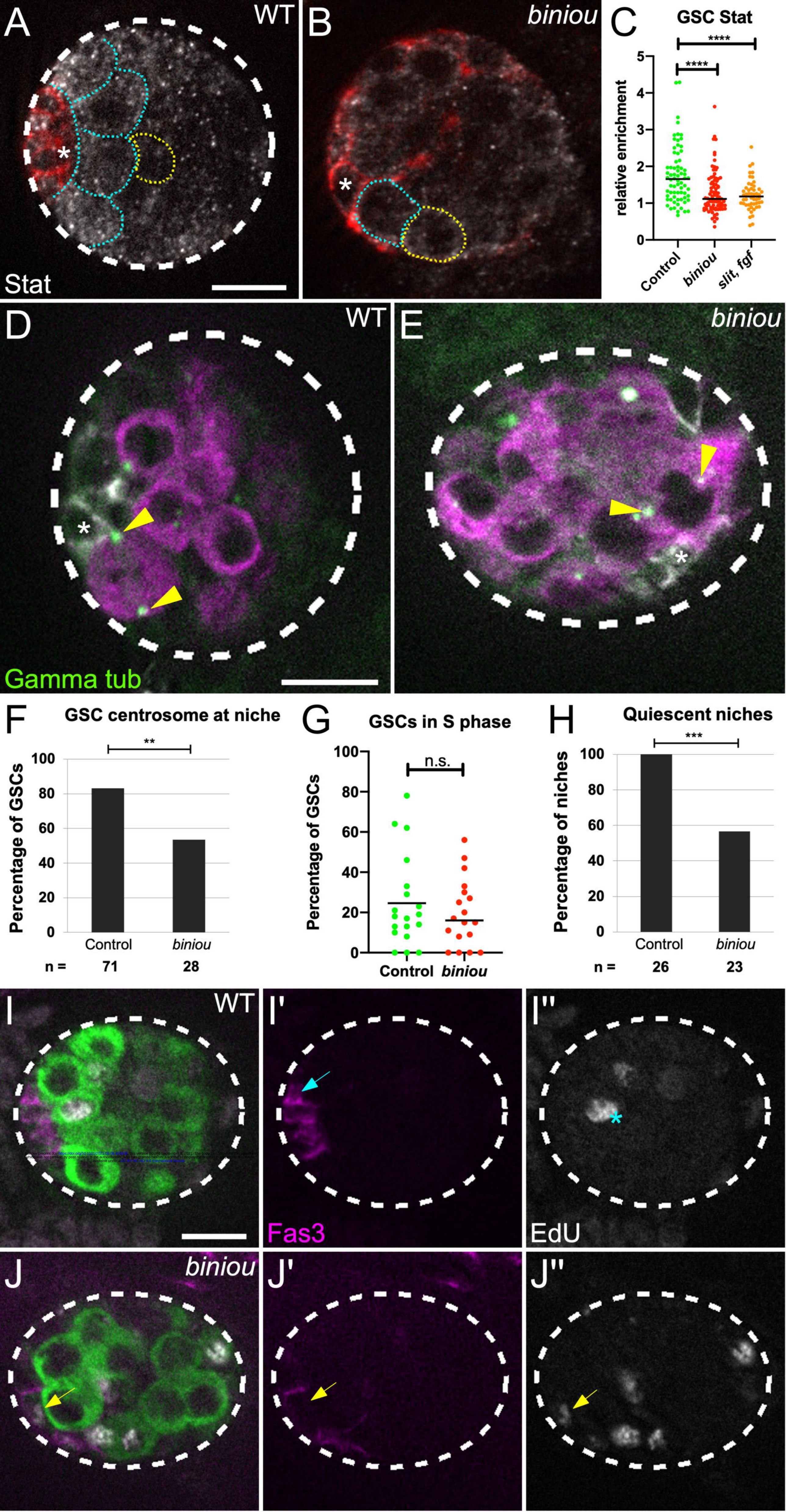
A
WT
Stat
B
biniou
C
GSC Stat
****
****
relative enrichment
0
1
2
3
4
5
Control
biniou
slit, fgf
D
WT
Gamma tub
E
biniou
F
GSC centrosome at niche
**
Percentage of GSCs
0
20
40
60
80
100
Control
biniou
n =
71
28
G
GSCs in S phase
n.s.
Percentage of GSCs
0
20
40
60
80
100
Control
biniou
H
Quiescent niches
***
Percentage of niches
0
20
40
60
80
100
Control
biniou
n =
26
23
I
WT
I'
Fas3
I''
EdU
J
biniou
J'
J''

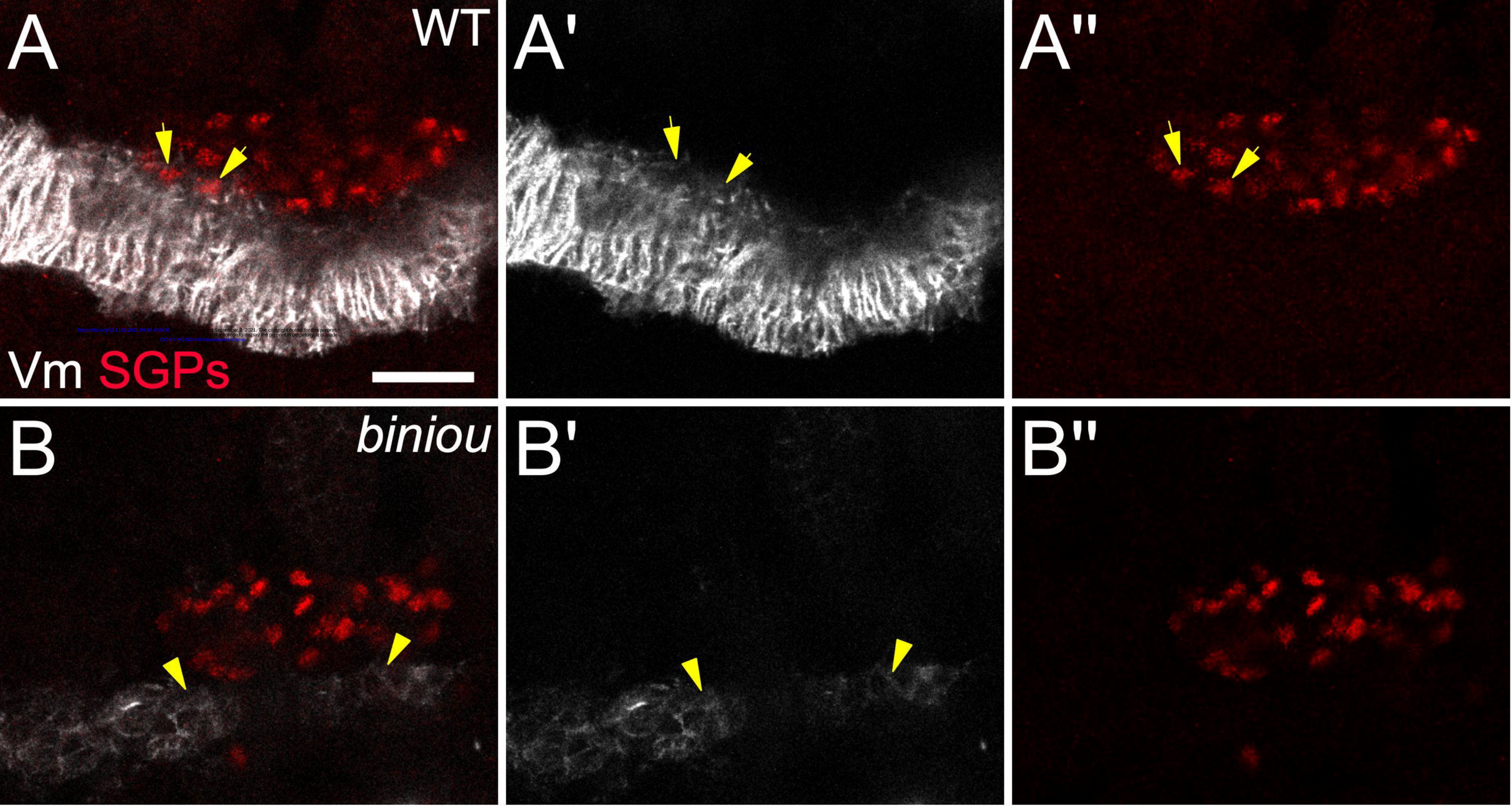

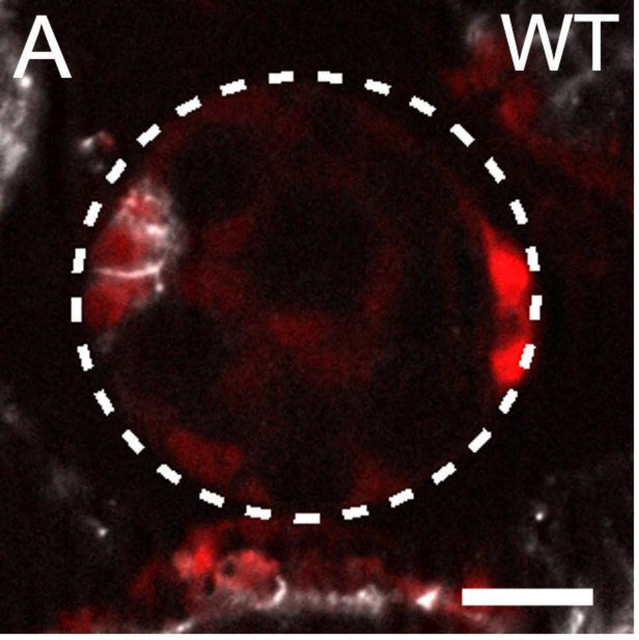

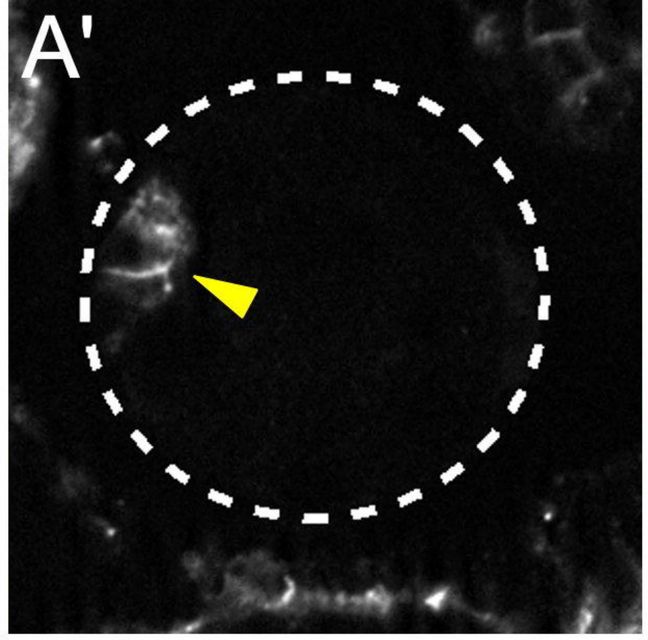

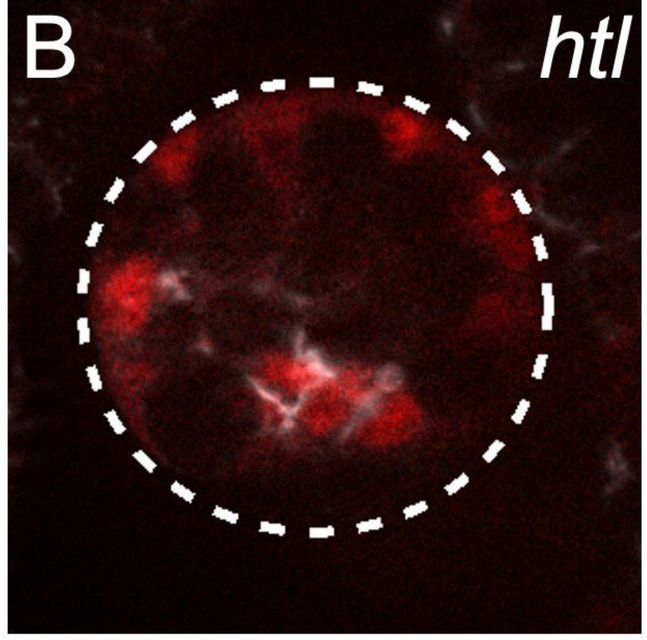

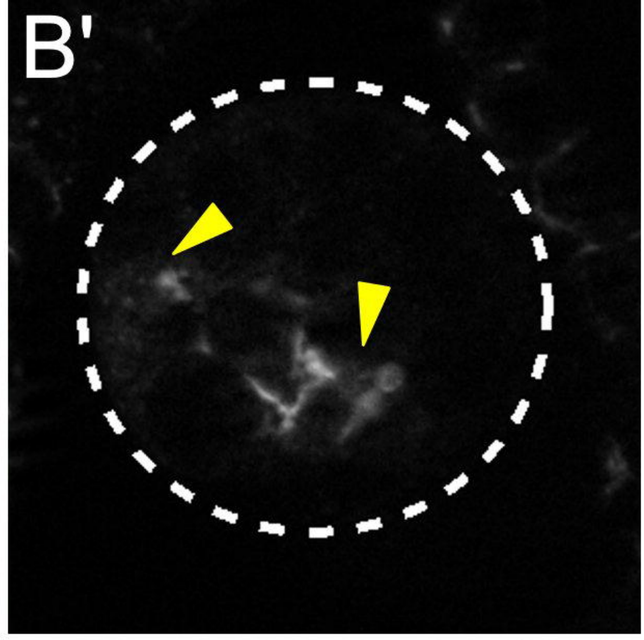

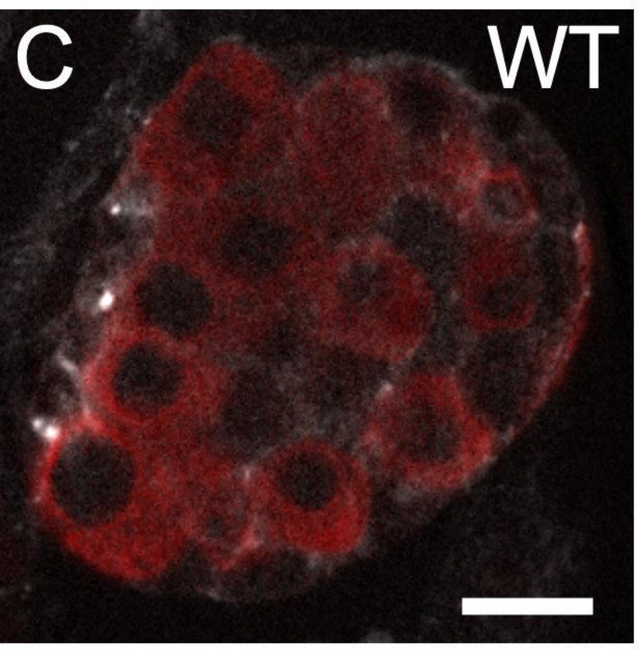

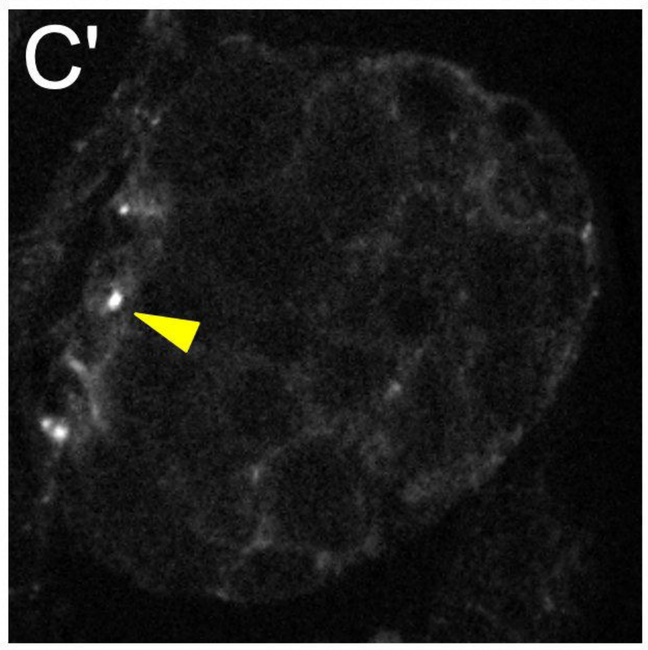

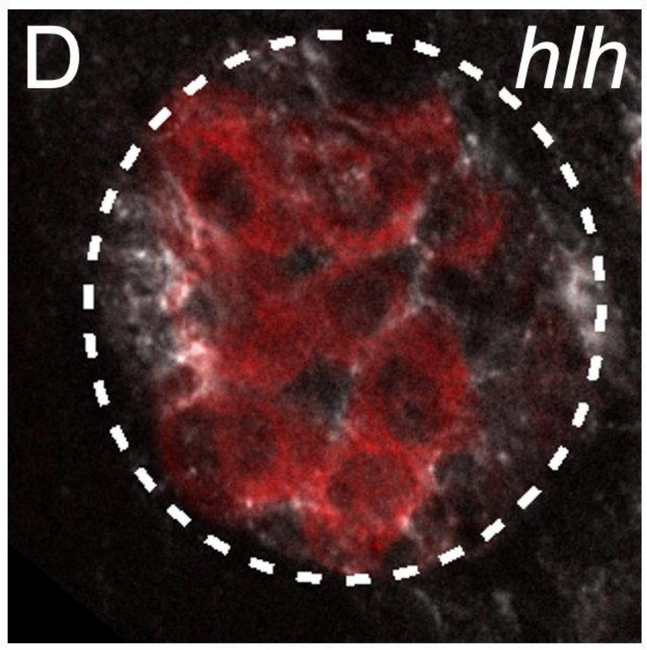

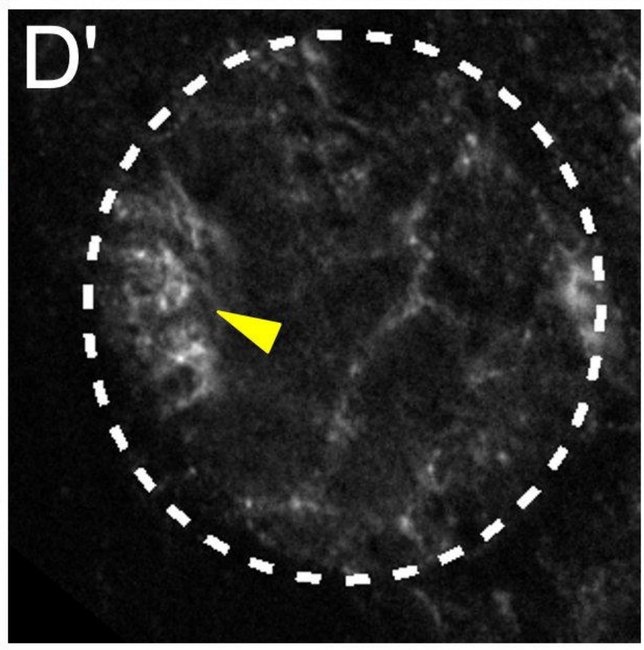

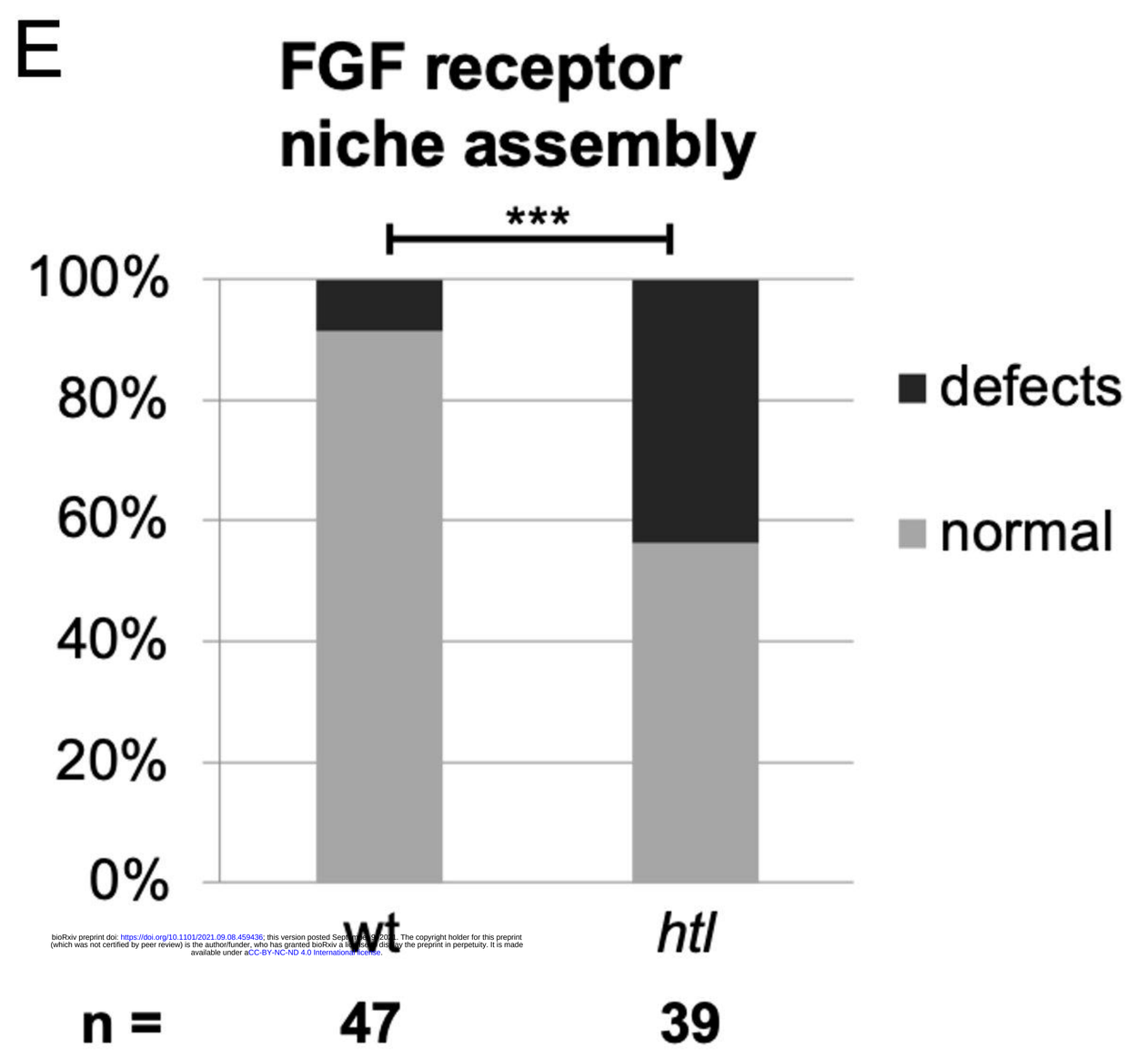

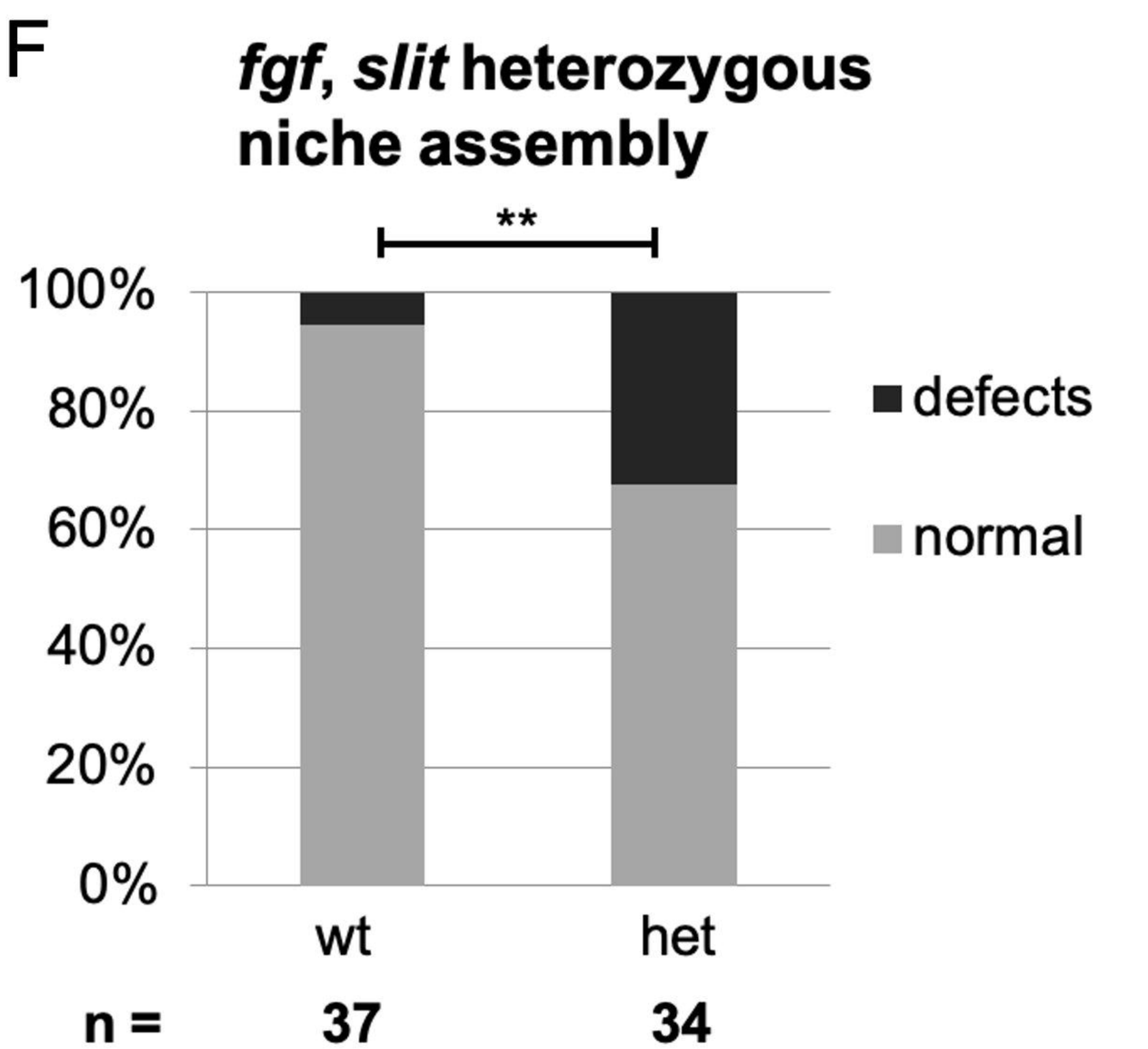

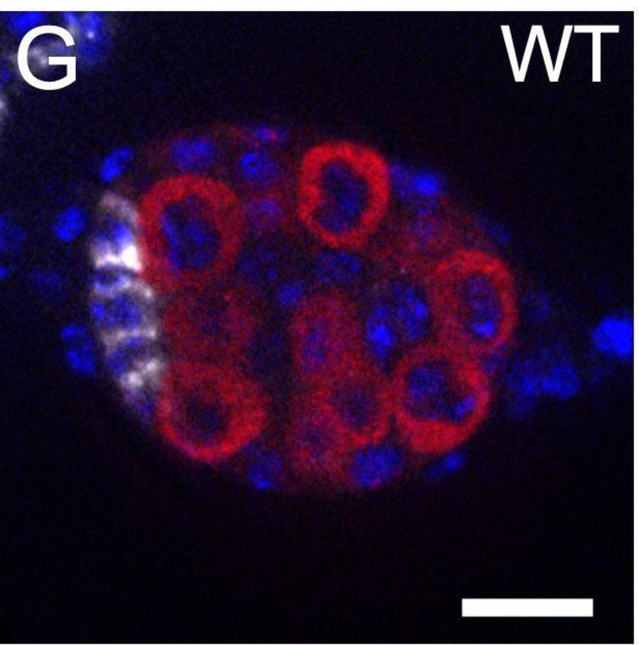

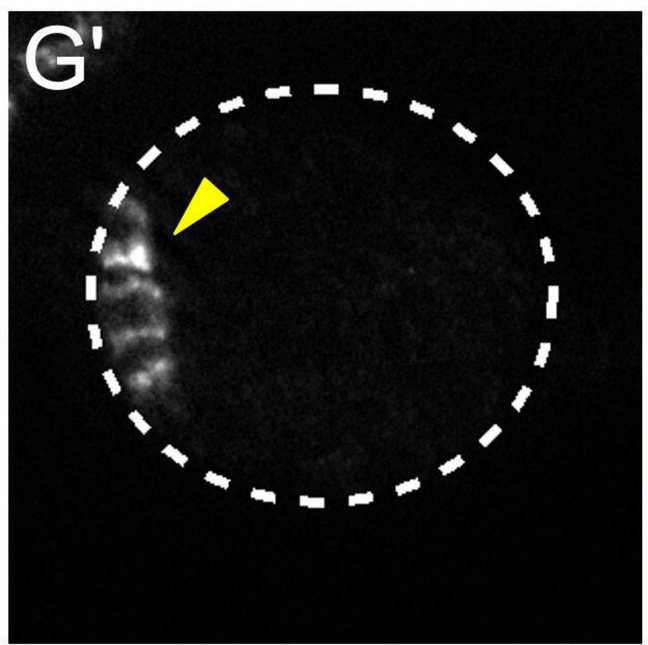

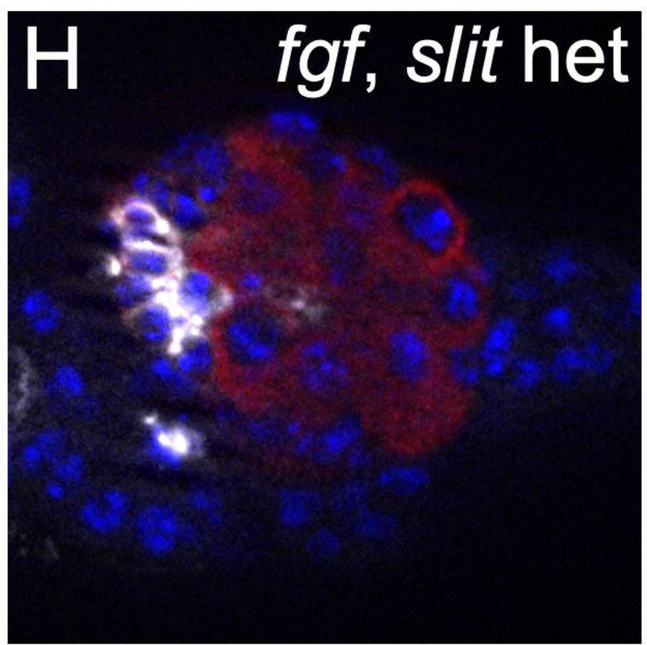

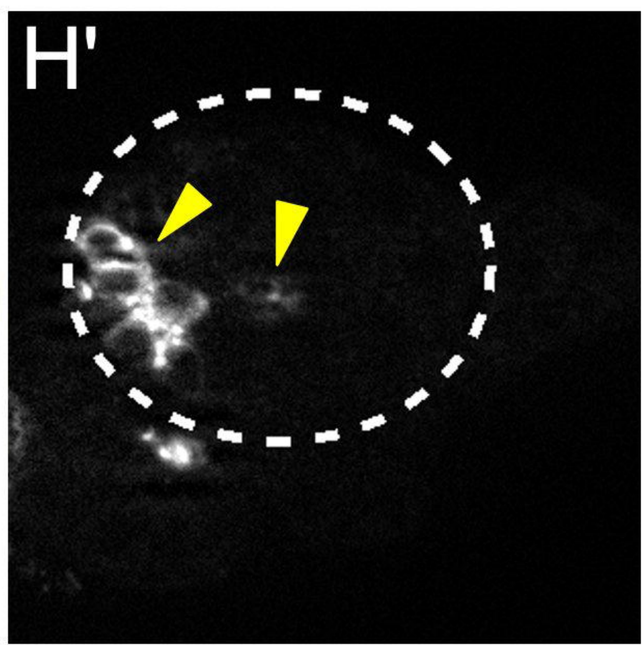

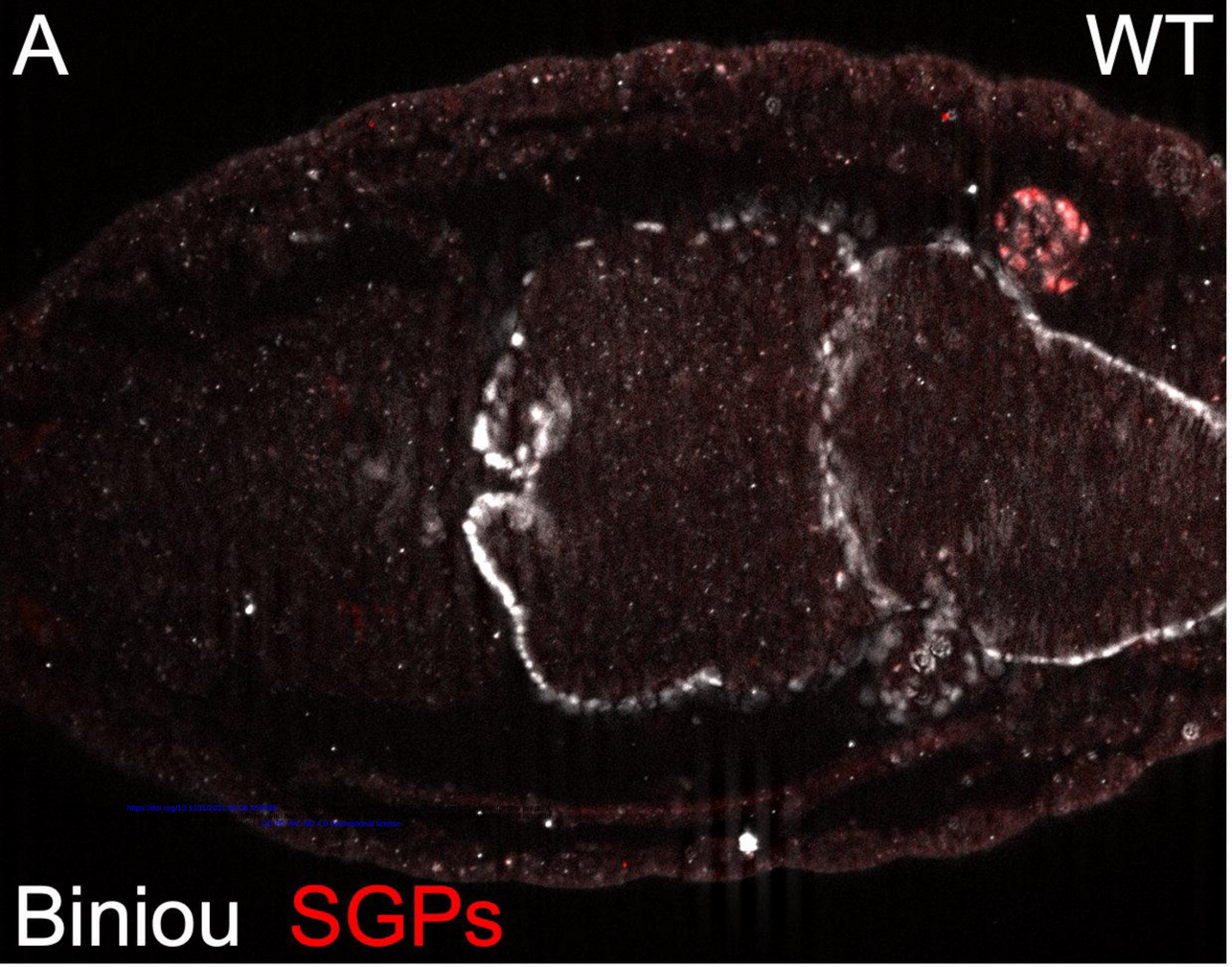

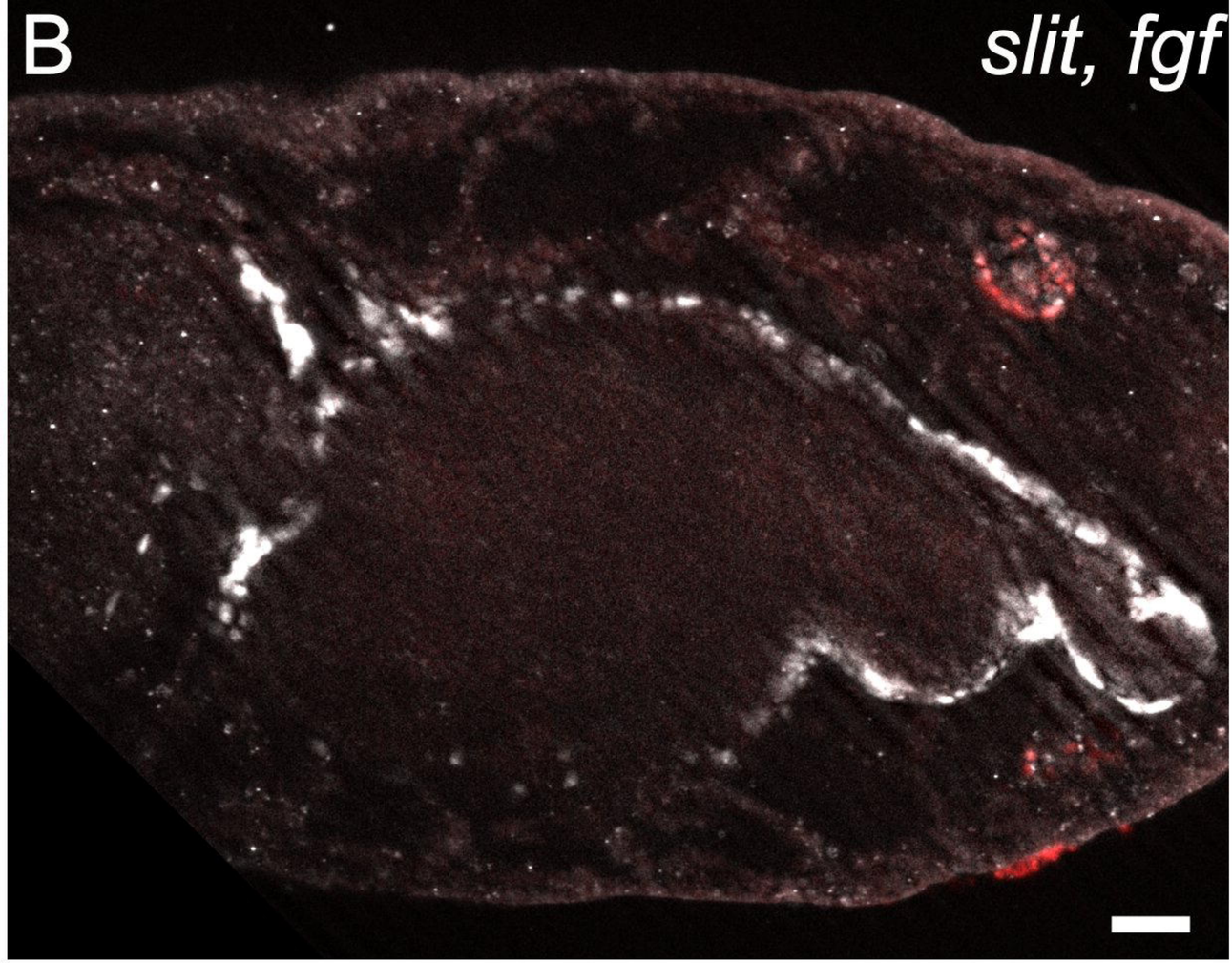

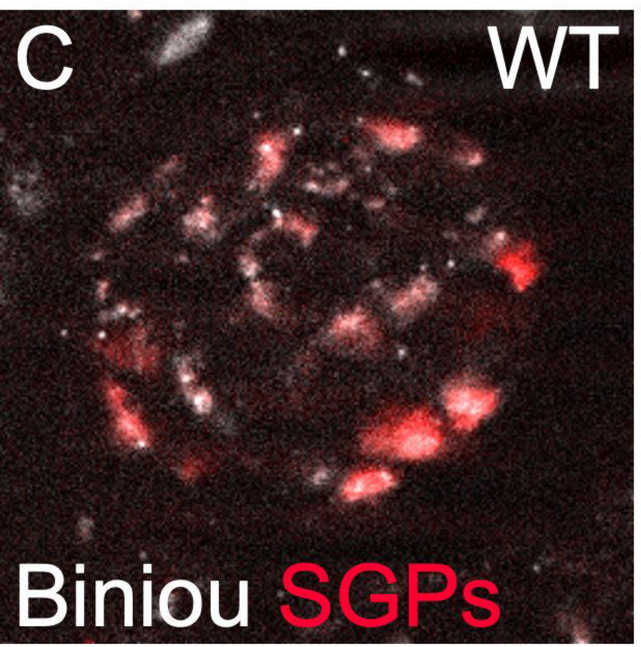

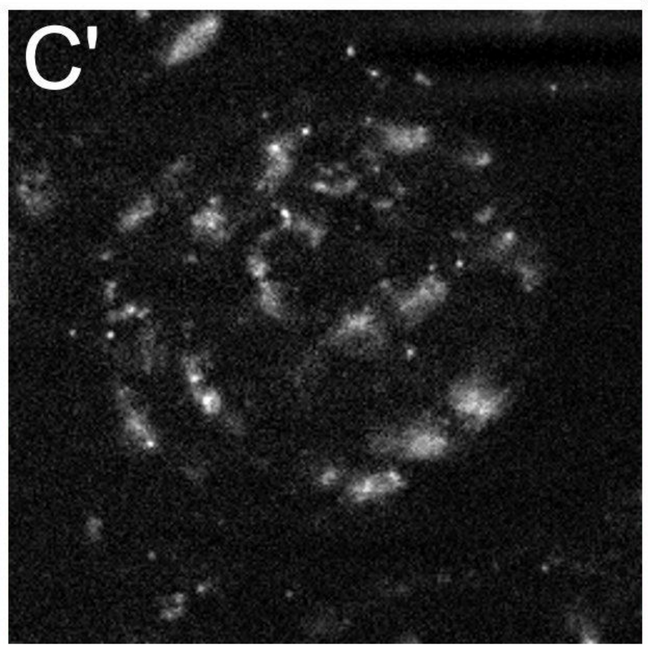

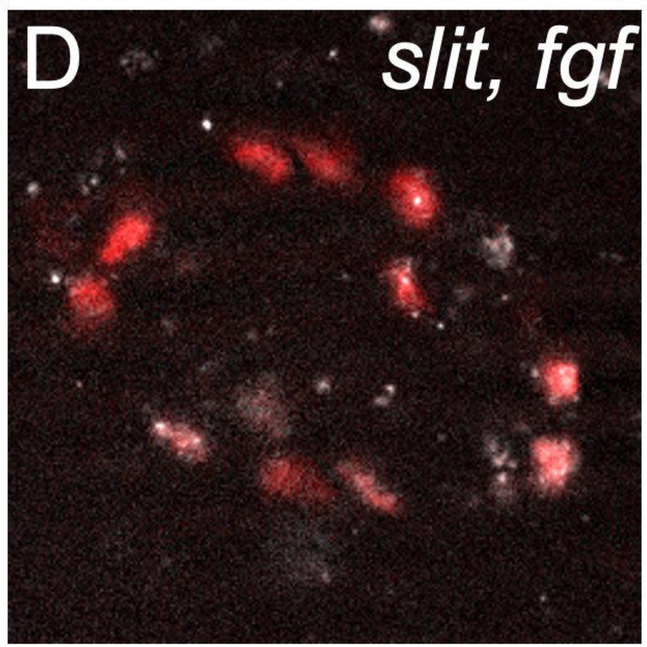

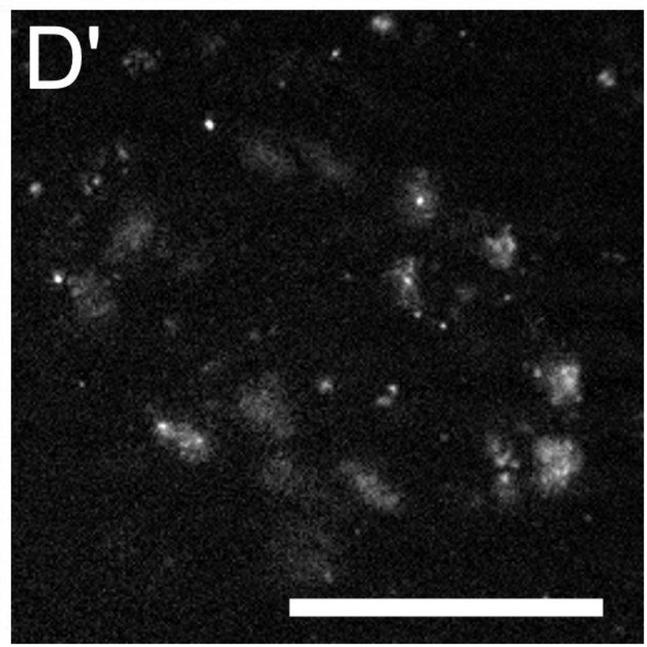

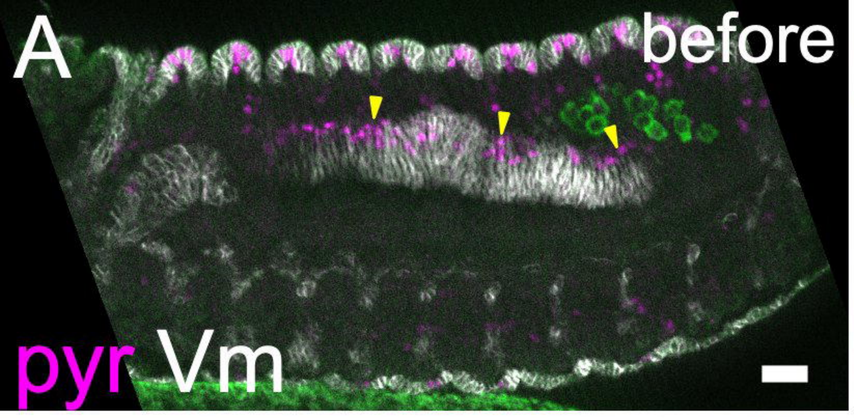
A
before
pyr Vm

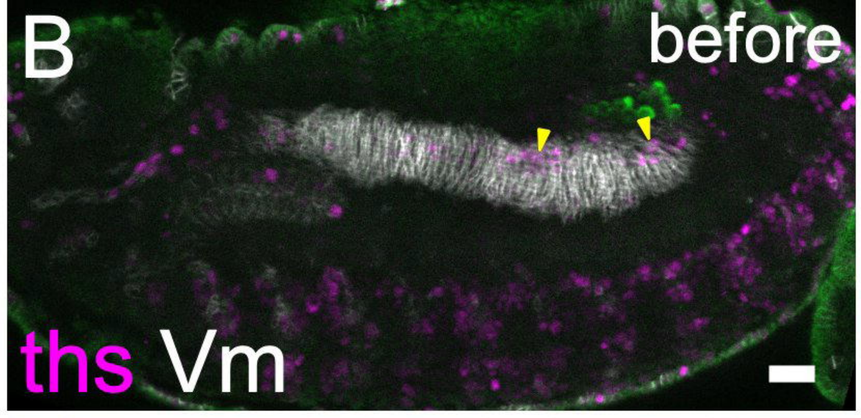
B
before
ths Vm

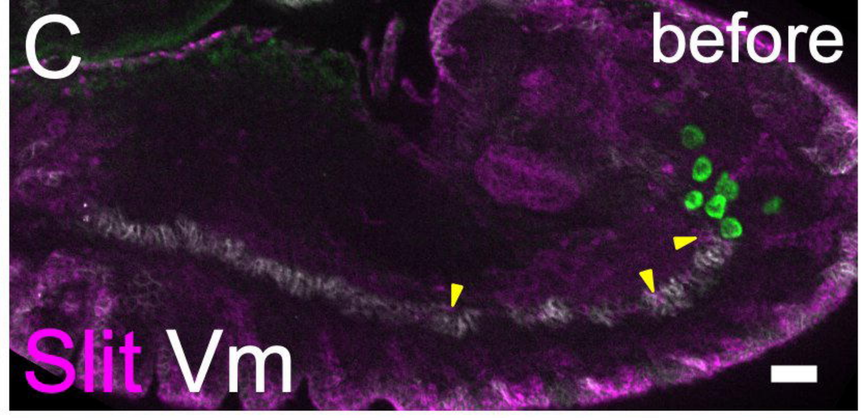
C
before
Slit Vm

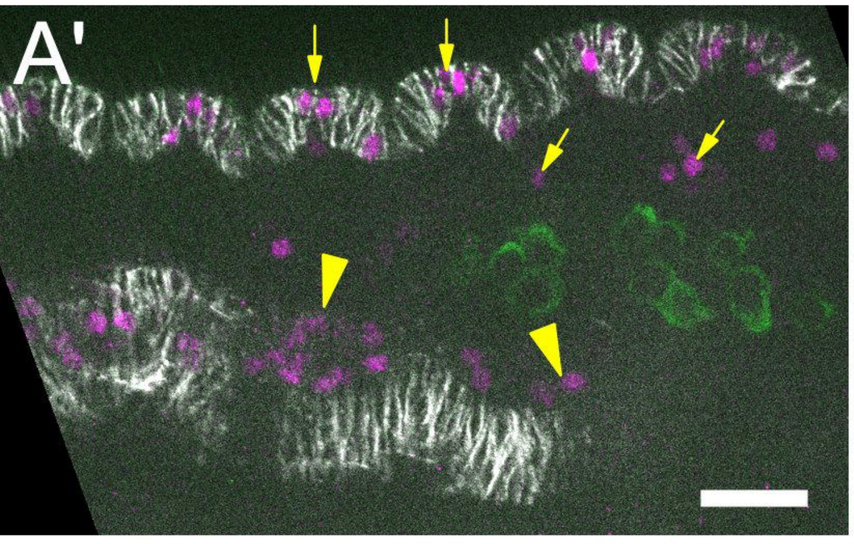
A'

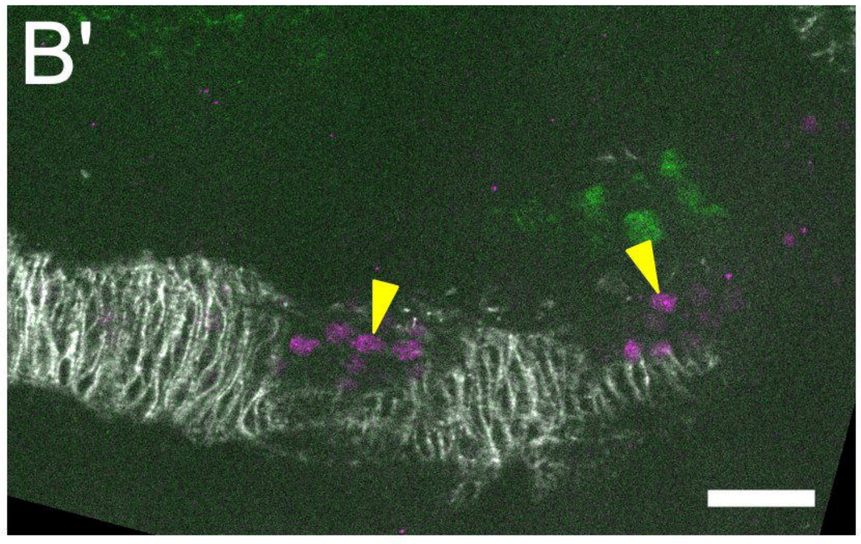
B'

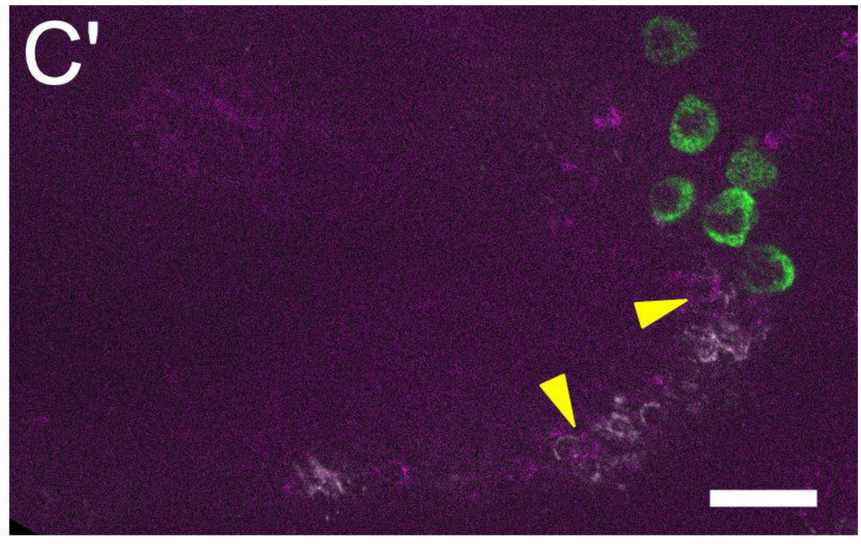
C'

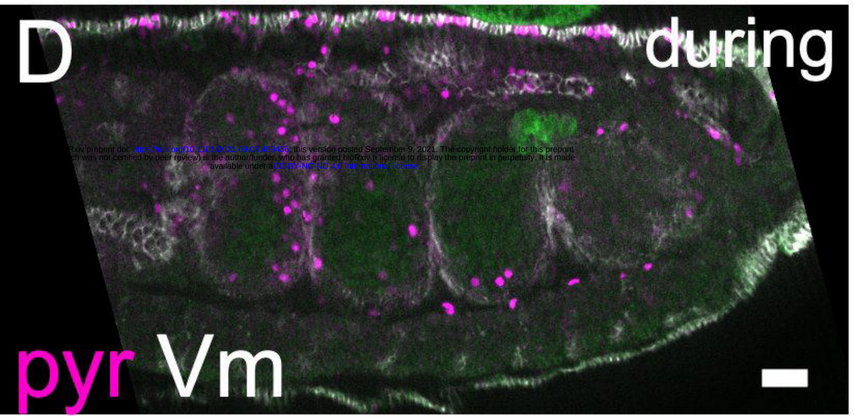
D
during
pyr Vm

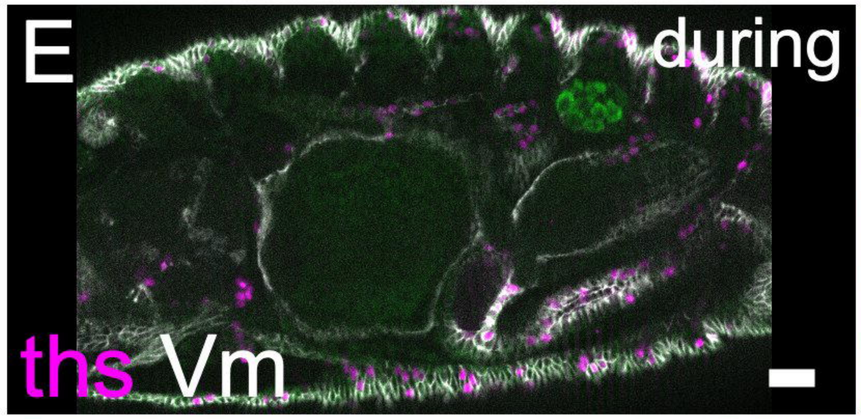
E
during
ths Vm

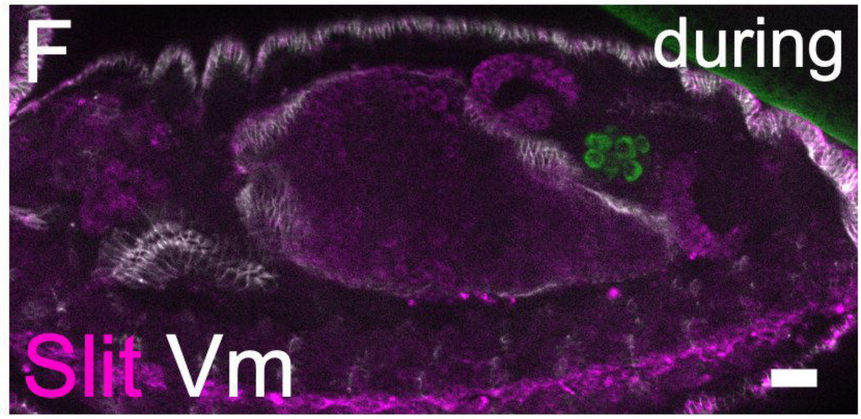
F
during
Slit Vm

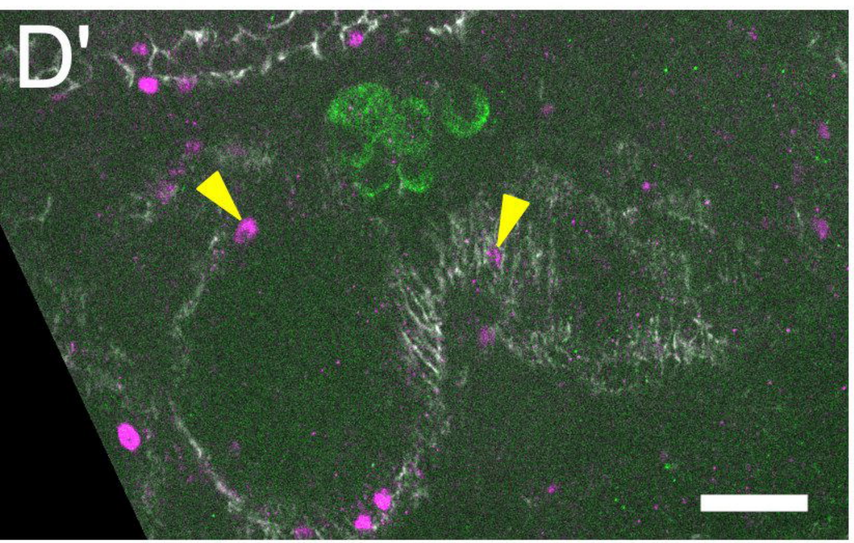
D'

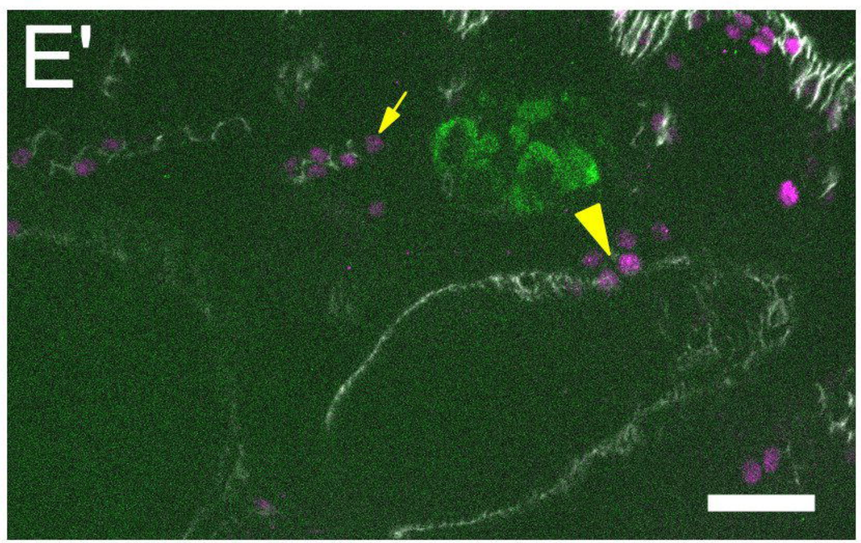
E'

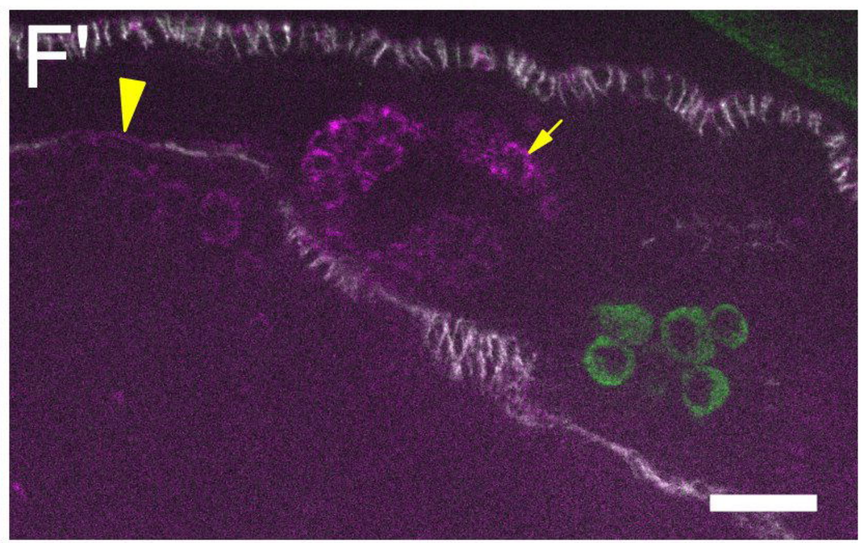
F'